

Debris-flow dominance of alluvial fans masked by runoff reworking and weathering



Tjalling de Haas^{a,*}, Dario Ventra^a, Patrice E. Carbonneau^b, Maarten G. Kleinmans^a

^a Faculty of Geosciences, Utrecht University, PO-Box 80115, 3508 TC Utrecht, The Netherlands

^b Department of Geography, Durham University, DH1 3LE Durham, UK

ARTICLE INFO

Article history:

Received 14 November 2013

Received in revised form 23 April 2014

Accepted 25 April 2014

Available online 6 May 2014

Keywords:

Alluvial fan

Secondary processes

Stratigraphy

Atacama

Mars analog

UAV imagery

ABSTRACT

Arid alluvial fan aggradation is highly episodic and fans often comprise active and inactive sectors. Hence the morphology and texture of fan surfaces are partly determined by secondary processes of weathering and erosion in addition to primary processes of aggradation. This introduces considerable uncertainty in the identification of formative processes of terrestrial and Martian fans from aerial and satellite imagery. The objectives of this study are (i) to develop a model to describe the sedimentological and morphological evolution of inactive fan surfaces in arid settings, and (ii) to assess the relative importance of primary processes of aggradation and secondary processes of weathering and reworking for surface morphology and sedimentology and for the stratigraphic record. We studied an alluvial fan characterized by a recently active sector and a long-abandoned, inactive sector along the coast of the hyperarid Atacama Desert. Here, rates of primary geomorphic activity are exceptionally low because of extreme aridity, while weathering rates are relatively high because of the effects of coastal fogs. Long-term processes of fan aggradation and reworking were determined through sedimentological facies analysis of stratigraphic sections. Ground surveys for textural and morphological patterns at the fan surface were integrated with remote-sensing by an Unmanned Airborne Vehicle (UAV). Discharges and sediment-transport capacities were calculated to estimate the efficiency of secondary runoff in reshaping the inactive fan sector. Stratigraphic sections reveal that the fan was dominantly aggraded by debris flows, whereas surface morphology is dominated by debris-flow signatures in the active sector and by weathering and runoff on the inactive sector. On the latter, rapid particle breakdown prevents the formation of a coarse desert pavement. Furthermore, relatively frequent local runoff events erode proximal debris-flow channels on the inactive sector to form local lag deposits and accumulate fine sediment in low-gradient distal channels, forming a well-developed drainage pattern that would suggest a runoff origin from aerial images. Nevertheless, reworking is very superficial and barely preserved in the stratigraphic record. This implies that fans on Earth and Mars that formed dominantly by sporadic mass flows may be masked by a surface morphology related to other processes.

© 2014 Elsevier B.V. All rights reserved.

1. Introduction

Alluvial fans are prominent depositional landforms at the transition between highlands, which provide debris sources, and adjacent basins that offer long-term sediment accommodation (Harvey, 2010). One fundamental goal of alluvial fan research has been to link fan surface features with formative processes (e.g., Hooke, 1987; Whipple and Dunne, 1992; Blair and McPherson, 1998; Gómez-Villar and García-Ruiz, 2000; Blair, 2002; Volker et al., 2007). However, whereas many kinds of subaerial processes and their related landforms are observable over different time scales, alluvial fans pose particular challenges to direct interpretation. While aggradation of these landforms occurs from highly episodic runoff and mass-flow events and often concentrates on an active lobe comprising a small area of a fan surface, most of the time fans are

subject to secondary processes of weathering and erosion by fluvial and/or aeolian activity, which may have a significant effect on the final morphology of these landforms (Blair and McPherson, 1994, 2009). For example, in arid environments weathering and erosion progressively reduce clast size and relief on long-abandoned fans resulting in the development of desert pavements and subdued, incised surfaces (e.g., Wells et al., 1987; McFadden et al., 1989; Ritter et al., 1993; Al-Farraj and Harvey, 2000; Matmon et al., 2006; Frankel and Dolan, 2007).

A fan surface is dominated either by primary processes of deposition or by secondary processes that modify the original depositional morphology. Which of these processes dominate depends on the balance between the characteristic time scales to cover and build morphology by primary deposition and to modify morphology by secondary processes, here expressed as a morphological factor M :

$$M = \frac{T_{\text{deposition}}}{T_{\text{modification}}} \quad (1)$$

* Corresponding author. Tel.: +31 30 2532778.

E-mail address: t.dehaas@uu.nl (T. de Haas).

wherein $T_{\text{deposition}}$ is the time needed for an initial surface to become entirely covered by a primary deposit, and $T_{\text{modification}}$ is the time scale required for secondary processes of weathering and erosion to remove or modify the typical morphology of primary deposits. The morphology of fans with $M > 1$ is dominated by primary processes of deposition, whereas surfaces with $M < 1$ are dominated by secondary processes, which do not cause significant aggradation. For example, Blair and McPherson (1994) suggested that the origin of many alluvial fans may have been misinterpreted because of secondary reworking of original surface morphology. This mainly applies to alluvial fans with low recurrence intervals of depositional events and high rates of reworking, but without significant net aggradation by secondary processes. Because of the potentially misleading surface morphology and texture, the origin of such alluvial fans should ideally be inferred from stratigraphic sections that provide independent evidence for the dominant processes of long-term fan formation. The question is then to what extent the surface morphology reflects the primary process of fan formation. This needs to be unraveled for application to remote terrestrial and planetary alluvial fans that can only be interpreted from satellite imagery.

The objective of this study is to determine the relative importance of debris flows and fluvial reworking on alluvial fan surface morphology and texture and stratigraphic record. Specifically we aim to (i) construct a conceptual model of arid fan surface evolution after abandonment; (ii) compare our specific example to those of other terrestrial arid environments; and (iii) assess the implications of fan surface modification by weathering and fluvial reworking for the aerial recognition of fan formative processes on Earth and on Mars.

We analyze this on a fan along the Pacific coast of the hyperarid Atacama Desert in northern Chile (Fig. 1), where average rates of primary geomorphic activity are exceptionally low (e.g., Dunai et al., 2005; Nishiizumi et al., 2005). The fan shows a distinctly bipartite morphology, with a proximally incised active sector flanked by long-abandoned, inactive sectors enabling the comparison of the effect of primary versus secondary processes through an active fan surface where $M > 1$ and an inactive fan surface where $M < 1$.

Complementary sources of information were combined. First, we used sedimentological analyses of incised sections and surface deposits to independently identify dominant processes of long-term fan aggradation as well as the genetic characterization of different morphosedimentary facies at the surface. This provided the evidence to distinguish between primary processes of fan aggradation and secondary processes of surface reworking. Second, remotely sensed hyperspatial imagery with <10 cm resolution (see Carbonneau et al., 2012) was obtained to study spatial patterns of morphology, texture, and sorting calibrated by surface sediment sampling. We created maps of median particle size (D_{50}) and digital elevation (DEM), which we used to quantify textural and morphological differences between the active and inactive fan sectors with emphasis on two different secondary processes: weathering and fluvial reworking. Third, we calculated flow and sediment-transport capacity to evaluate the potential of runoff in reshaping the inactive fan sector. Finally, we combined the results obtained from these complementary approaches to propose a conceptual model for surface evolution after abandonment. The paper is organized as follows. First we describe the general geological and climatic setting of the study location followed by the detailed methods. We then compare the active and inactive sectors of the fan in sedimentological analysis followed by the surface morphology and texture analyses, after which we propose a model for fan surface evolution by primary and secondary processes. The discussion focuses on comparison to other arid environments and implications for inference of primary process from imagery on Earth and on Mars.

2. Geological and climatic setting

The Coastal Cordillera of northern Chile is a prominent topographic feature extending more than 700 km along the active tectonic margin between the oceanic Nazca Plate and the continental South American

Plate (Armijo and Thiele, 1990; Hartley et al., 2005). Owing to crustal thickening and uplift, the Cordillera has an average altitude of 1000 m and locally reaches elevations in excess of 2000 m above sea level, forming a steep escarpment that terminates with precipitous slopes onto the Pacific coast. The dominant lithologies of the Cordillera are Jurassic andesites and associated granitic intrusions (Ferraris and Di Biase, 1978; Hartley et al., 2005), which feed steep colluvial systems and numerous alluvial fans at the base of the coastal escarpment, as well as discontinuous shoreline deposits.

The hyperarid Atacama Desert region has extremely low precipitation rates that average <5 mm/y between 18° and 24°S (Houston and Hartley, 2003), and no precipitation is commonly recorded over many consecutive years. The major source of humidity along the Atacama Desert coast is the camanchaca, a recurrent coastal fog condensed from subsiding warm air along the eastern margin of the SE Pacific Anticyclone that interacts with the cold Humboldt Current near sea level (Araveni et al., 1989; Marchant et al., 2007). In general, the coastal fogs are prevented from reaching far into the continental interior as they are commonly entrapped along the oceanward margin of the Coastal Cordillera (Hartley et al., 2005). Because of the near absence of precipitation, alluvial depositional events are very rare in the Atacama Desert. Near Antofagasta, depositional events are estimated to have occurred approximately once every 210 years between 5 and 1 Ka, and once every 40 years over the last thousand years (Vargas et al., 2006). However, seven debris-flow events are recorded in Antofagasta between the years 1916 and 1999 (Vargas et al., 2000), and several studies linked geomorphically effective floods to severe El Niño events in the Atacama region (e.g., Vuille, 1999; Vargas et al., 2000, 2006; Houston, 2006).

Salt-weathering is the dominant weathering mechanism in the Atacama Desert (Berger, 1993; Berger and Cooke, 1997; Goudie et al., 2002). Along the Coastal Cordillera, salts are deposited mostly by condensation of the camanchaca and, to a lesser extent, are blown landward by winds from the ocean. The camanchaca contains considerable amounts of dissolved salts, mainly nitrates (Eriksen, 1981) and sulfates (Schemenauer and Cereceda, 1992). Large quantities of salts combined with the prolonged inactivity of geomorphic surfaces form an ideal precondition for pervasive salt-weathering, particularly effective on loose debris at the surface of coastal fans (Berger, 1993; Berger and Cooke, 1997; Hartley et al., 2005).

Fans along the Atacama Desert coast are predominantly formed by debris flows, but colluvial cones and fluvial surfaces do occur (see Hartley et al., 2005; de Villiers, 2013, for descriptions of fans in the larger area). We selected a fan (Fig. 1) with an area of 1.05 km² and a maximum width of 950 m. Fan slope is ~11° at the apex and generally declines to ~6° near the fan toe. The average slope is 8.3°, the apex is located at 247 m above sea level, and the fan toe terminates into the Pacific. The fan is fed by a steep catchment with an area of 3.42 km² and a maximum height of 1204 m above sea level conveying runoff from the Coastal Cordillera toward the Pacific. Bedrock in the catchment mainly consists of Jurassic andesites of the La Negra Formation (Ferraris and Di Biase, 1978). Pedogenic cover and vegetation are completely absent owing to the extreme local aridity.

The fan surface can be divided into two distinct morphosedimentary domains because of a large incision at the apex (Figs. 1, 2): (i) a relatively young sector formed by relatively recent depositional events ($M > 1$), flanked by (ii) two older sectors that have undergone a long period of depositional inactivity, while being exposed to secondary processes of weathering and erosion for a prolonged period ($M < 1$). The younger sector has a maximum distal width of 250 m and comprises ~25% of the total fan surface.

3. Methods

We assessed primary aggradational processes on the fan by sedimentological analyses of incised sections and characterized patterns of surface morphology and texture by combining a ground survey with hyperspatial

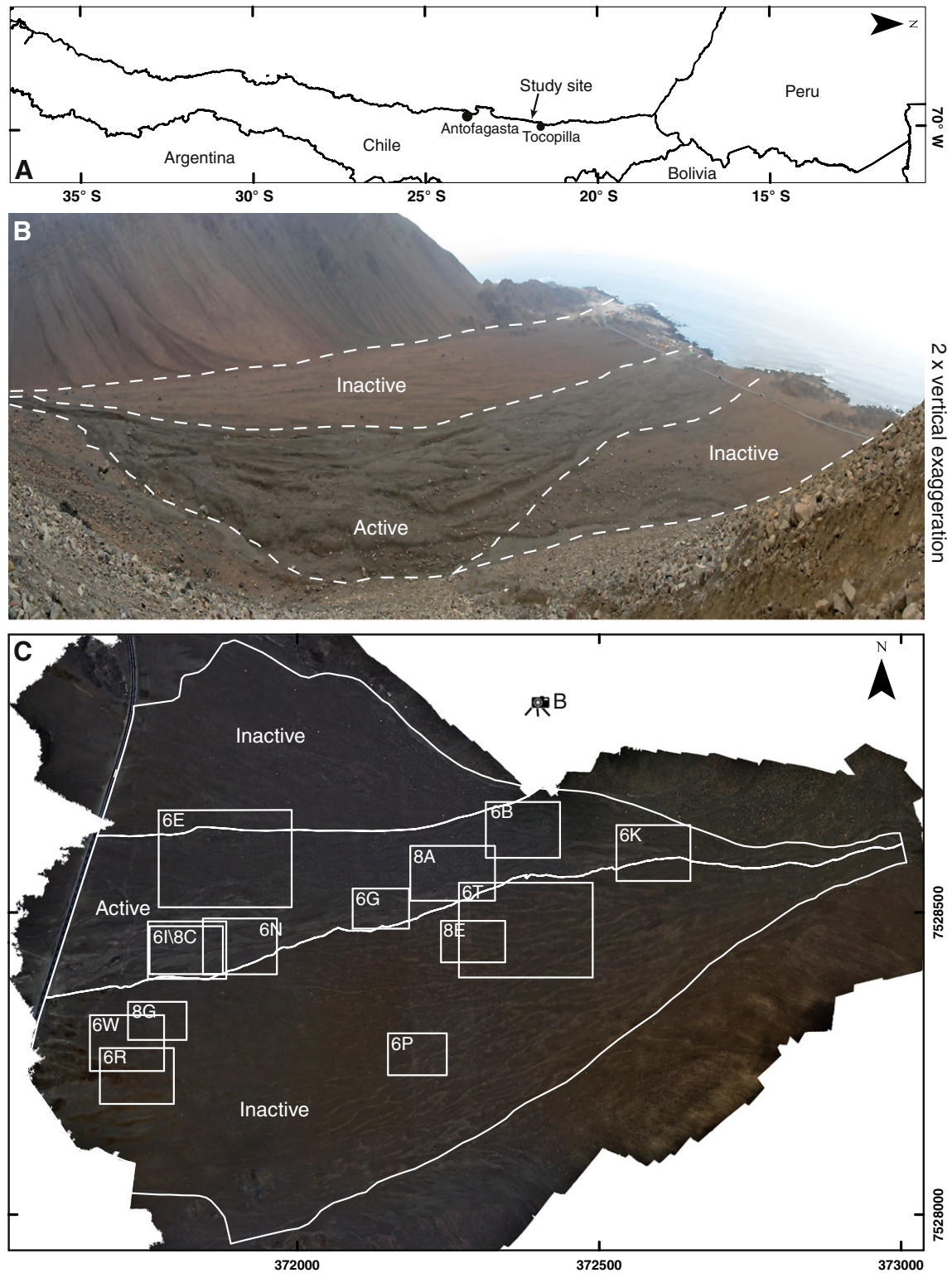


Fig. 1. Location and overview of the study area. (A) Location of studied fan centered at 22°20'42"S, 70°14'33"W, with coordinates in UTM WGS84 19 S (grid-spacing: 500 m). (B) Panoramic image indicating active and inactive sectors. Image is vertically stretched for visibility. (C) Orthomosaic showing the active and inactive sectors. Boxes indicate locations of panels in Figs. 6 and 8.

imagery collected with an Unmanned Aerial Vehicle (UAV). Below we explain data collection, processing and data reduction methods.

3.1. Field survey

The dominant processes of long-term fan aggradation were identified by sedimentary facies analysis along dip-oriented stratigraphic

sections up to 3 m in depth exposed along the main incised channels of the fan. Dominant depositional and reworking processes were determined by geomorphological field reconnaissance and by mechanical and photosieving of sediment at selected locations for quantification of surface textures (detailed later). Different categories of deposits were identified over the fan surface based on distinctive geometry and on textural, fabric, and architectural characters. Each category was

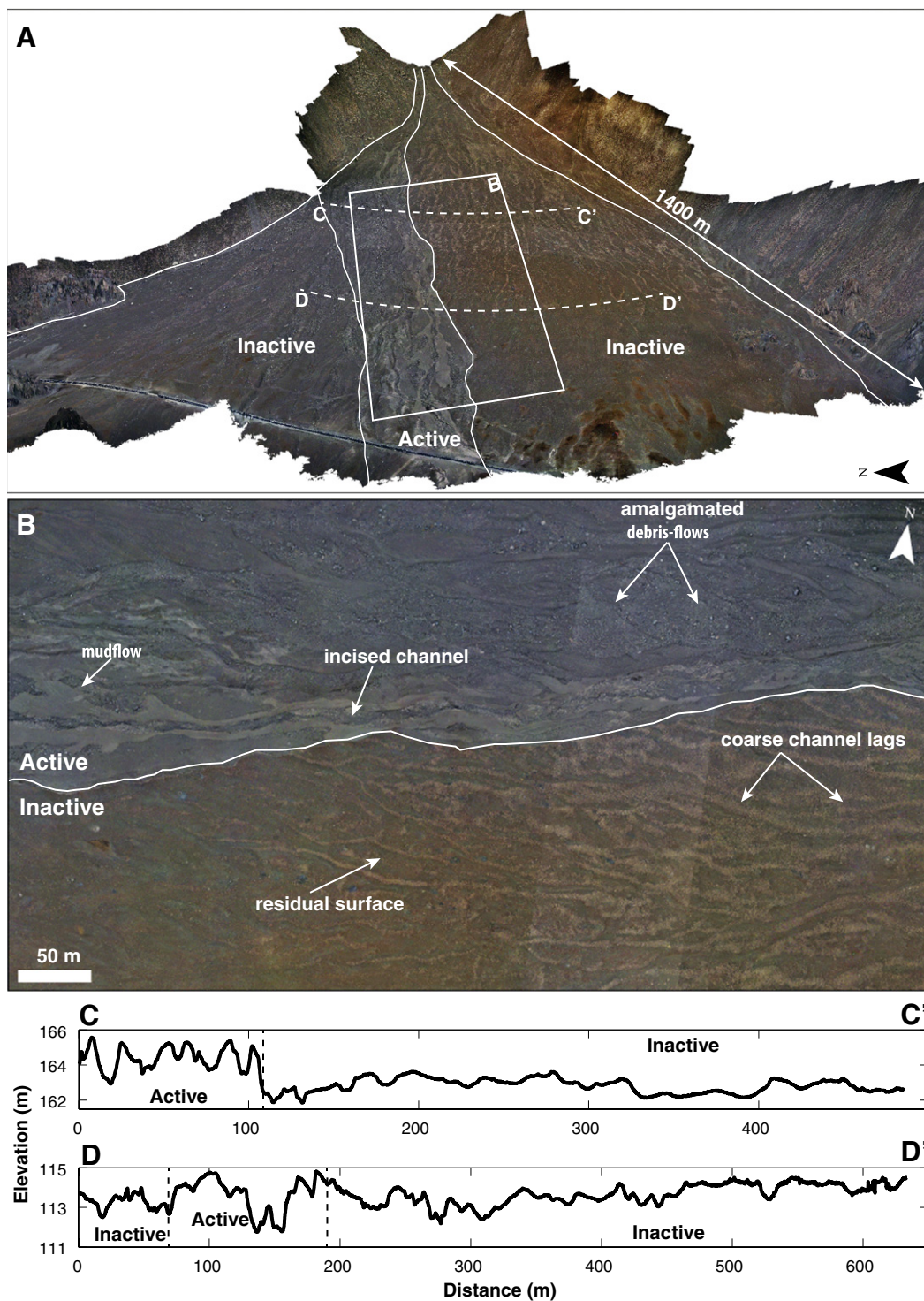


Fig. 2. Active and inactive sectors on the fan. (A) Three-dimensional view of the fan in true colors, indicating the active and inactive lobes. Box indicates location of panel B. (B) The terminator between the active and inactive sectors with typical morpho-sedimentary deposits. (C) Topographic cross-section of the proximal domain. (D) Topographic cross-section of the distal domain.

associated to a distinct process of sedimentation and/or reworking, allowing for the recognition of genetically distinct facies (hereafter termed 'morphological facies').

3.2. UAV image acquisition

Remotely sensed imagery of the fan surface was obtained by means of a SmartPlanes SmartOne Unmanned Aerial Vehicle (UAV), which is a lightweight system (1.1 kg) with a wingspan of 1.2 m. It

carries a small format Canon Ixus RGB camera with a 7-megapixel sensor. It is equipped with an infrared navigation system and on-board GPS that enables autonomous flight and controlled image acquisition. Images were taken at elevations of 125–175 m above the fan surface. Because the UAV flight control software does not account for local topography when flying in proximity to the steep valley walls, altitude had to be increased to prevent an impact with the surrounding relief. The image spatial resolutions varied from 4 to 6 cm.

Flights were carried out during late mornings, between ~09:00 and 11:00 A.M., under clouded sky conditions but in the absence of fog. These conditions were found to be locally optimal because the presence of strong sunshine combined with the funnel-like topography of the fan valley led to very strongly upwelling thermal currents, which made UAV control extremely difficult and unsafe. In total, over 2200 images were acquired.

Many images were affected by various levels of relative motion blur, which was an inevitable consequence of the cloudy conditions that reduced light levels and increased exposure times. Furthermore, a few images were blurred as a result of wind gusts that jarred the UAV. Motion blur is a function of altitude and instantaneous velocity; because the UAV was not equipped with accelerometers, a quantitative approach to motion blur correction could not be adopted nor could quantitative selection criteria be established. Therefore we subjectively removed the most blurred images. In order to maintain full coverage of the fan, some minor blur was tolerated and this left 1969 images.

Images were processed with *Agisoft Photoscan* software (Agisoft, 2011), which uses Structure from Motion (SfM) in a photogrammetric workflow with very high levels of automation and good levels of data quality (e.g., Fonstad et al., 2013). Following the standard SfM-photogrammetry workflow, a point-cloud comprising 49.39 million vertices was produced. The point cloud was then georeferenced to UTM map coordinates with 26 ground control points (GCPs) surveyed with a ProMark 3 dGPS. This dGPS system works in static acquisition mode. Control point positions were logged for 10 min and then differentially corrected with respect to a fixed base station installed at the distal margin of the fan, <1 km from any point. The dGPS point accuracy ranged from 3 to 12 cm. The GCPs were first used to optimize the point-cloud model and minimize optical distortions in the model.

This optimization process also allowed us to register the point-cloud to map coordinates. In SfM-photogrammetry, registration to map coordinates proceeds with a rigid 7-parameter transform that scales, rotates, and translates the point cloud. The parameter values in the transformation are determined in a least-squares sense from the GPC coordinates. This implies that any nonlinear distortions present in the topography can no longer be removed. With the point-cloud registered, the covered fan area comprised 0.745 km², which yields an average point density of 66.3 points/m².

3.3. DEM production from UAV imagery

The point cloud was rasterized in order to produce DEMs in a standard, regular-grid format. The highest resolution DEM had a spatial resolution of 10 cm. The quality of DEM was checked against the original GCPs. Given that the 7-parameter registration is rigid, these points have residuals. Based on these, the vertical accuracy of the DEM was found to be ~5.1 cm.

However, the RMSE between control points and DEM was found to be 1.95 m. Closer examination of the DEM clearly shows that this is not caused by surface noise and that these errors are not randomly distributed in space. Rather, the RMSE errors are associated to a small, gradual deformation affecting the whole DEM. A centered second-order polynomial fit of the residuals yielded strong second-order components of $-1.2x^2$, $1.268xy$, and $0.38y^2$ with an R^2 of 0.74. The deformation is near-zero at the center and maximal at the edges. Similar deformations that fit a polynomial surface were observed by the authors in the past. The vertical deformation amplitude represents 0.44% of the DEM half-length.

Over short scales, if we assume that the polynomial deformation is linear, this yields a maximum slope error estimate of 0.254°. These types of deformations in UAV DEMs derived from SfM-photogrammetry have not been well documented and are difficult to correct for in the absence of comprehensive LiDAR surveys, which would increase the cost of the work tenfold and in fact obviate the need for a UAV. We therefore decided to avoid any untested correction procedures and keep the DEM products unmodified, especially as a maximum slope error of 0.254° does not significantly influence our results.

The final step in the SfM-photogrammetry workflow is the production of orthoimagery. Here we produced orthomosaic products at a constant spatial resolution of 6 cm. Some residual, randomly distributed, blurred patches remained and were most likely caused by wind gusts.

3.4. Particle size map

The fan orthomosaic was used to produce a continuous surface particle size map. Carbonneau et al. (2004) and Carbonneau (2005) demonstrated that, in images of sediment particles, image texture correlates well to the median size of the particles. This approach does not rely on the precise delineation of particle boundaries, rather, it relies on variations of brightness values within a local area (33×33 pixels, 0.99×0.99 m, in Carbonneau et al., 2004). The underlying physical justification is that larger particles cast larger, but localized, shadows thus leading to more variation and light/dark contrasts. Consequently, this method requires an empirical calibration for each image data set. This calibration assumes that all pixels in the image have the same resolution and therefore it was essential to use the orthomosaic despite the slight blurring effects. For the first time we applied the method developed by P. Carbonneau et al. (2012) to the alluvial-fan environment. Here, a texture metric called entropy was calculated from the co-occurrence matrix (Haralick and Shapiro, 1985). This entropy is logarithmically proportional to the range of brightness values in an image neighborhood. It is therefore well suited for particle size mapping as the logarithm damps small variations in brightness because of natural color variations while remaining sensitive to large light/dark contrasts. For ground-truthing, 112 planview images of 12 megapixels were taken on the fan surface at locations covering the entire range of particle sizes present on the fan. Each image covered a rectangular frame of 1.0×0.75 m laid over the surface. The northeast corner of the frame was surveyed by dGPS to pinpoint the position of close-range photos on the airborne ones. Particle size distributions on close-range photos were calculated via photosieving after correction for lens distortion and oblique camera orientations to the surface, using the rectangular frame for scale. For each photo, the long and intermediate axes (a and b , respectively) of 100 clasts were measured at 100 random positions plotted on the image. Particles with b -axes smaller than 3 pixels were below the methods resolution and were assigned a default size of 3 pixels (~0.3 mm). Particle b -axes were used to calculate a probability density function by number. We used the arithmetic particle size distribution (Blott and Pye, 2001) to derive the D_{50} for entropy calibration.

Samples were collected at 32 photo locations for mechanical sieving to produce geometric particle size distributions. For comparisons we converted the arithmetic particle size distributions (by number) from the photosieving to geometric distributions (by weight), assuming spherical particles with diameter b and converting the sphere volume to weight, assuming constant mass density for all size fractions. Comparison of the 16, 50, and 84 percentiles shows acceptable agreement (Fig. 3), but photosieving tends to overestimate the particle size for fine-grained samples because of the resolution limit. Entropy calculated at ground-truth image locations and median particle sizes from photosieving were correlated by linear regression. Here the dimensionless ψ -scale median particle size is defined as $\psi = \log_2(D_{50}/D_{ref})$, where D_{50} is the median particle diameter and $D_{ref} = 1$ mm is the reference diameter. Entropy was calculated on a 64-level grayscale image of the orthomosaic. Blurred sections in the orthophoto artificially reduce entropy; therefore, 25 out of 112 ground-truth locations that fell within these sectors were omitted from the calibration. The window size was 10×10 pixels (0.70×0.70 m), which resulted in the clearest pattern in optimization tests in the range 5×5 to 40×40 pixels. The least squares linear relation between entropy E and particle size ψ , with $R^2 = 0.82$, is (Fig. 4)

$$\psi = -2.35E - 2.98. \quad (2)$$

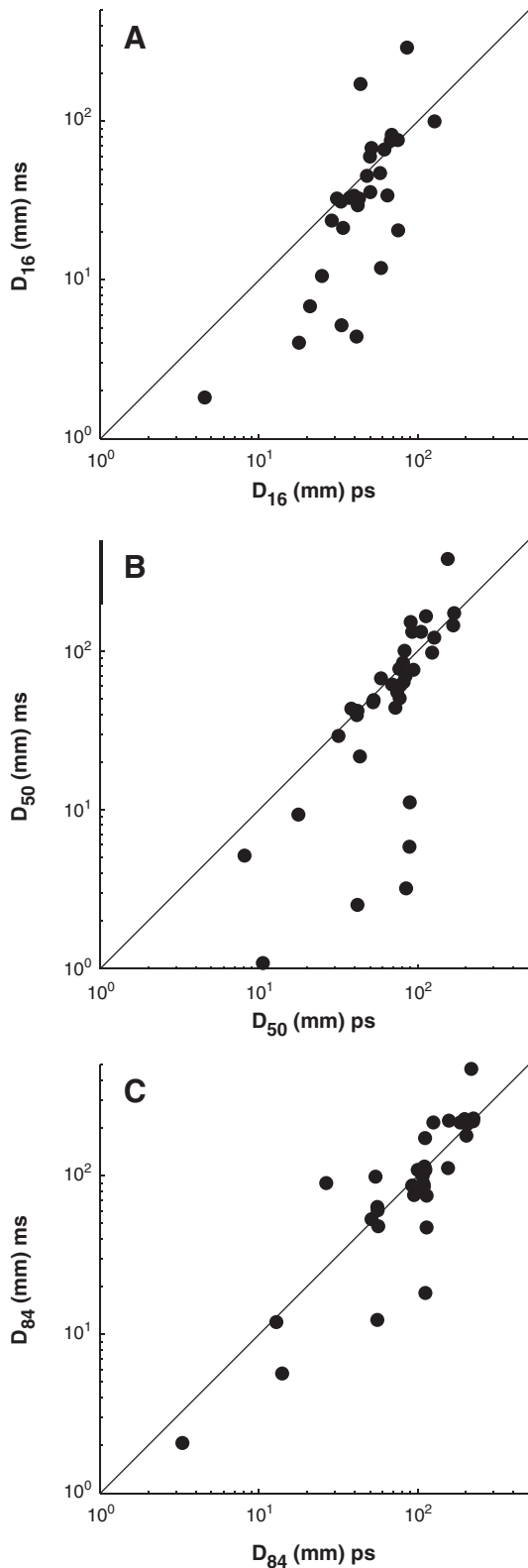


Fig. 3. Comparison between photosieving (ps) and mechanical sieving (ms) for geometric particle size percentiles. (A) D_{16} , (B) D_{50} and (C) D_{84} .

3.5. Data reduction

Down-fan trends on the active and inactive sectors were assessed for elevation, detrended elevation, surface roughness, and particle size. Detrended elevation was calculated by subtracting a smoothed DEM from the original DEM. The smoothed DEM was calculated from median

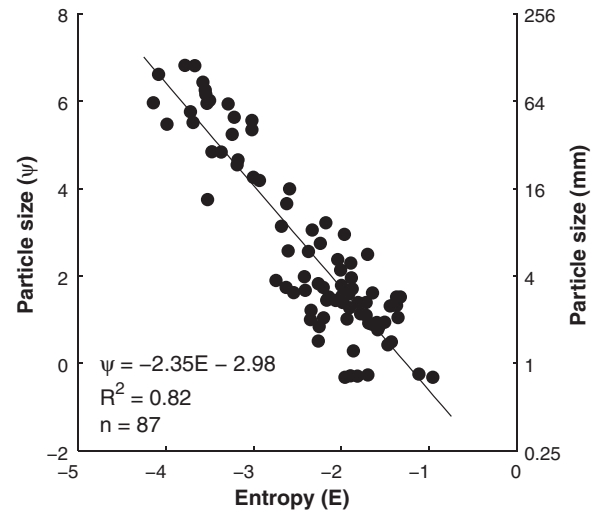


Fig. 4. Empirical relation between image entropy E in the aerial imagery and arithmetic median particle size derived from photosieving in the field. Locations were exactly matched by GPS and context images.

filtering with a moving circular window with a 10-m radius to remove local relief of bar and swale morphology with typical wavelengths of 5 to 10 m that are commonly observed in arid alluvial environments (Frankel and Dolan, 2007). To quantify the degree of surface smoothing on the inactive fan surface, surface roughness was quantified by the standard deviation of the slope in a 5×5 m area (Frankel and Dolan, 2007).

Textural patterns were analyzed by quantifying the particle size distribution for each morphological facies on the active and inactive sector of the fan. To do so, representative areas were selected on the proximal and distal domain of these sectors. Locations of these areas were arbitrarily selected such that they comprised all the morphological facies, and image blur was minimized. Because the locations were restricted to relatively blur-free areas, the size of the representative areas varies slightly. This does not significantly influence the results as the size of the representative areas is much larger than the spatial resolution of the grid cells, so that a large population of values are used for each evaluated parameter. In the selected areas, the morphological facies were defined by visual interpretation, and the DEM constrained by ground truth. The median particle size of each grid cell within a morphological facies was extracted, along with values of detrended elevation. These values were then displayed in two-dimensional boxplots in order to compare the particle size distribution and the detrended elevation within the morphological facies.

Down-fan trends were assessed by extracting the values of elevation, detrended elevation, surface roughness, and particle size on circle segments centered at the fan apex at regular intervals of 1 m and calculating the median and quartiles of these values. We only plot data of the active sector and the southern inactive sector because on the northern active sector multiple recent debris flows occurred that originated from the steep slope adjacent to the fan. This pollutes the data of surface relief, roughness, and particle size from a different source than the rest of the fan, and therefore this sector was excluded from the analysis. Later verification showed that the unaffected areas on the northern inactive sector had similar values of surface relief, roughness, and particle size as the southern inactive sector.

To evaluate the effect of slope on secondary erosional and depositional patterns on the inactive fan surface, we calculated the mobility (Shields number) of various particle sizes over a range of slopes and compared this to the critical Shields number for incipient motion. The Shields number is defined as

$$\vartheta = \frac{\tau}{(\rho_s - \rho)gD_{50}} \quad (3)$$

where ρ_s = sediment density (2650 kg m^{-3}), ρ = water density (1000 kg m^{-3}), g = gravitational acceleration (9.81 m s^{-2}), and τ is the bed shear stress (N m^{-2} or Pa) calculated as

$$\tau = \rho g h \sin(S) \quad (4)$$

wherein h = mean water depth (m), and S = energy slope of the flow. The critical Shields number for incipient motion was calculated by the model of Vollmer and Kleinhans (2007), which corrects for steep slopes and shallow flow depth. Here the median particle size is considered representative for the entire mixture of sediment and indicative of average behavior for partial transport conditions. This holds in particular for unimodal sediments that are in equal mobility (Kleinhans and van Rijn, 2002) which we assume here for lack of detailed process observations.

4. Results

This section first discusses processes of long-term fan aggradation as interpreted from facies analyses of stratigraphic sections (Section 4.1). We then identify and describe the morphological facies on the basis of a morphosedimentary analysis of the active (Section 4.2.1) and inactive fan sectors (Section 4.2.2). Next, large-scale textural patterns over the fan surface and textural patterns for individual morphological facies are analyzed. Down-fan trends in elevation, detrended elevation, surface roughness, and particle size provide an overview of patterns on the full fan scale (Section 4.3). The effect of slope on fluvial reworking on the inactive sector is evaluated by analyzing sediment mobility (Section 4.4). Finally, we combine all results to provide a conceptual model for fan surface evolution after abandonment (Section 4.5). The relation between formative process, stratigraphic facies and morphological facies is summarized in Table 1.

4.1. Processes of long-term fan aggradation

Three sedimentologically distinct facies can be recognized within the stratigraphic sections on the proximal sector of the fan (Fig. 5): debris-flow deposits (facies DF), fluvial runoff deposits (facies FF), and gravel lags of fluvial erosive origin (facies EF). Based on the relative volumetric abundance of the identified facies, the studied fan aggraded dominantly by stacking of coarse, poorly sorted, debris-flow sheets and lobes (~85–90% by visual estimation in stratigraphic sections). This means that the system can be classified as a debris-flow fan (Blair and McPherson, 1994). The minor volume of runoff-related facies FF and EF (~10–15%) indicates that floods merely redistribute sediment on the fan surface and that their contribution to primary aggradation is insignificant at system scale. Below we detail the sedimentological observations that support these interpretations.

Facies DF, interpreted as debris-flow deposits, consist of very poorly sorted, matrix- to clast-supported pebble to fine boulder gravel in beds continuous over meters to a few tens of meters along sections, varying in thickness from a few decimeters to ~1.5 m. Depositional facies are parallel to subparallel to the sloping fan surface, with subplanar bases showing little or no erosion, whereas bed tops may include isolated or clustered outsized clasts. Beds commonly present no grading or weak inverse grading; no preferential fabrics have been observed in the gravel

fraction, with clasts generally oriented randomly in a poorly sorted, silty to sandy matrix. The broad granulometric range of deposits, outsized gravel clasts and lack of erosive topography underneath flow units point to deposition by debris flows, with substantial yield strength and laminar flow behavior (e.g., Fisher, 1971; Hubert and Filipov, 1989; Blair and McPherson, 1998).

The upper boundaries of debris-flow beds occasionally show moderately to well-sorted, clast-supported cobble gravel (facies EF), occurring in discontinuous lenses with erosive bases into underlying debris-flow units (Fig. 5B,E). Most are one to a few clasts thick (20–30 cm), a few meters wide, and internally structureless or crudely layered. Platy and elongated gravel clasts show weak imbrication, but grading or fabrics are not evident. The superposed and weakly erosive position into the debris-flow units suggests an origin by winnowing, scouring, and armoring of debris-flow deposits (Blair and McPherson, 1998; Blair, 1999), likely by dilute debris-flow tails or runoff generated by rainstorms. Selective entrainment of the fine fractions produced a poorly sorted lag of residual gravel with generally weakly developed fabrics for coarse pebbles to fine cobbles. The thickness of lenticular units indicates protracted erosion, which likely occurred in persistent shallow rills that discharged several runoff events. The limited thickness of the gravel lenses relates to low stream power and the inherent self-limiting nature of the armoring process (e.g., Parker and Sutherland, 1990; Kleinhans and van Rijn, 2002). The discontinuity of the deposit on the upper boundaries of debris-flow beds is caused by the spatially fractionated distribution of runoff over the fan surface.

The waterflow deposits (facies FF) comprise distinctly bedded, clast-supported, pebble to cobble gravel in single or amalgamated beds and lenses with thickness variable from a few centimeters to a few decimeters (Fig. 5C,F). Most deposits feature moderate to very good sorting, well-developed imbrication, and tractive fabrics for nonspherical clasts. Thicker units present a distinct internal organization in planar divisions, evidenced by textural contrasts, while some units are characterized by absent grading and sheared fabrics with long clast axes oriented down-fan. A majority of beds comprise abundant sandy to granular matrix, often with fining-upward (normal) grading. Tractive sedimentary structures were not observed. Basal surfaces vary from nonerosive to distinctly erosive with scour up to a few decimeters. This indicates an origin by rapid deposition from shallow, unconfined to poorly confined waterflows in the occasion of major rainstorms. Relatively good sorting, normal grading, and the absence of tractive structures indicate deposition from bedload sheets (Whiting et al., 1988; Todd, 1996); flow-parallel fabrics and poorly developed structure point to ephemeral events of high sediment concentration, in which interparticle collisions prevented clast sorting and segregation in the shearing dispersion (Rees, 1968; Nemec and Muszynski, 1982; Todd, 1989).

4.2. Fan surface morphology

4.2.1. Active fan surface

The surface of the recently active fan sector is built up by gravel lobes and ridges of debris-flow origin (RGL), extensive mud lobes from very recent debris flows (RML), and a few incised, low-sinuosity channels (RFC) (Fig. 6A–N).

The gravel lobes and ridges of debris-flow origin (RGL) are most abundant on the surface. Lobes and ridges may be distinguishable as

Table 1
Relation between formative process, stratigraphic facies and morphological facies.

Process	Morphological facies		Stratigraphic facies
	Active sector	Inactive sector	
Debris flow	RGL: Gravel lobes from recent debris flows	IRD: Residual deposits from past debris flows	DF: Debris/mudflow
Mudflow	RML: Mud lobes from recent debris flows	IRD: Residual deposits from past debris flows	DF: Debris/mudflow
Runoff	RFC: Fluvial channels from recent runoff	ID: Eroded and filled depressions of local runoff	FF: Fluvial flow & EF: erosive fluvial flow

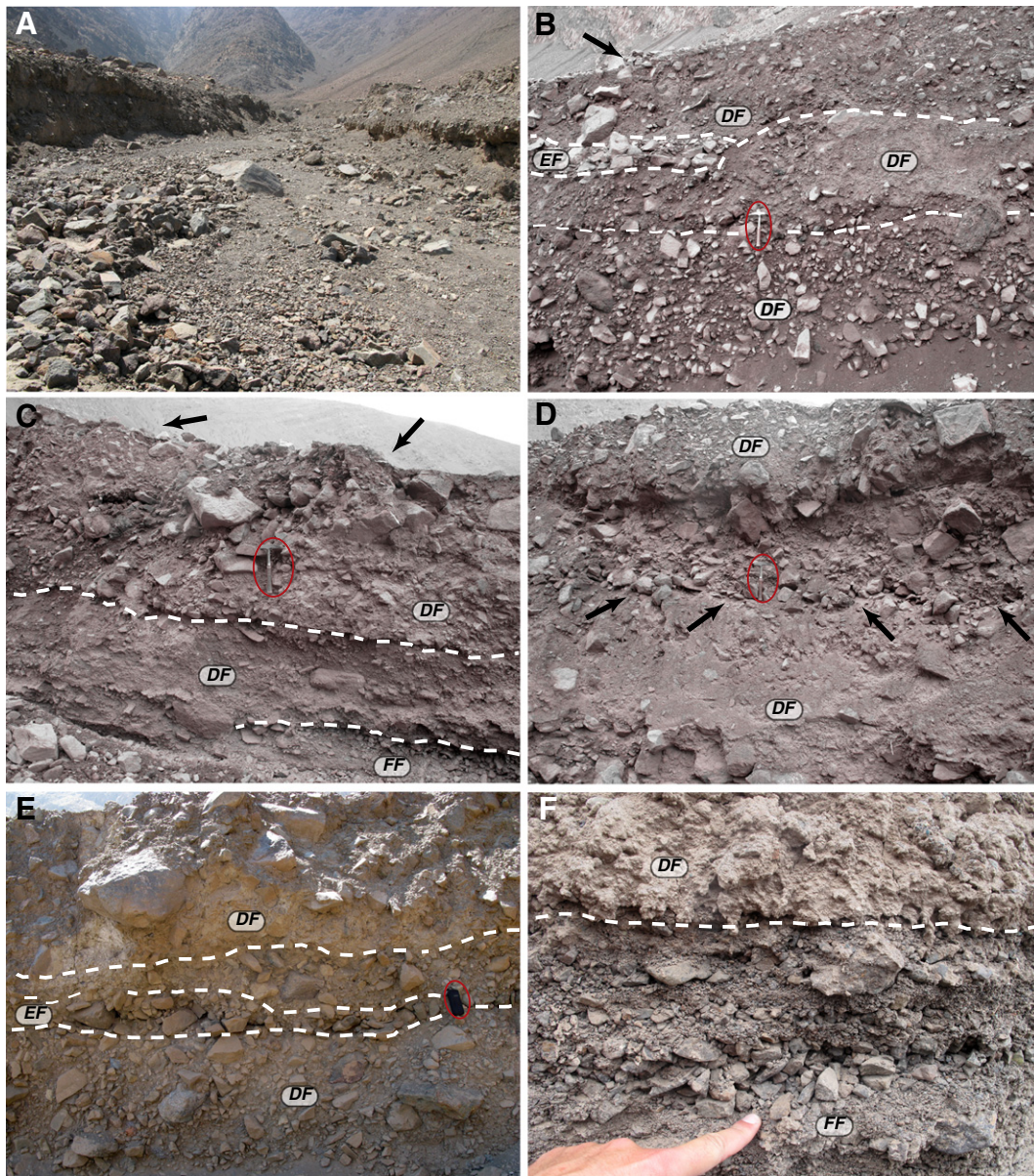


Fig. 5. Examples of sedimentary facies exposed in incisions on the proximal fan. Hammer, hand-held GPS and hand for scale. (A) The main incised channel close to the fan apex viewed up-fan. (B) Debris-flow deposits (facies DF) and a cobble-gravel lens (facies EF) formed by winnowing of fines. (C) Debris-flow deposits overlying waterlaid deposits (facies FF). (D) Debris-flow deposits. (E) Erosive cobble-gravel lens between debris-flow deposits. (F) Detail of a waterlaid deposit. Erroneous colors in panels B–D are due to camera error.

individual units by contrasting texture, weathering stage, varying topographic relief, segregated gravel ridges in lobes and levees and stepped topography at lobe margins. In general, they appear as a disorganized amalgamation of superposed and juxtaposed units (Fig. 6A–E). The majority of the surface sediment consists of angular, poorly sorted, pebble to boulder gravel, which is frequently clast-supported at the surface; a significant volume of silty to granule-grade matrix is retained a few centimeters below the surface. Boulders ranging in size from tens of centimeters to over 2 m in diameter occur randomly in the sediment and are partly exposed at the surface. Boulder frequency and relief of individual deposits decrease from the proximal to the distal fan sector as the more fluidal, finer-grained, and less cohesive debris flows mainly deposit on the distal fan sector (Fig. 6D,E) (Whipple and Dunne, 1992). Flow-parallel fabrics (Major, 1998) and segregations of coarser clasts into lateral levees and frontal snouts (Blair and McPherson, 1998; Johnson et al., 2012) can be identified in some of the individual lobes and ridges.

The mud lobes (RML) (Fig. 6F–E) were deposited as thin, cohesive, fine-grained debris flows (i.e., mudflows), which bypassed most of the fan and came to a halt on the low-gradient distal domain, possibly as late-stage, more fluidal phases of main debris-flow events (Pierson, 1986; Wells and Harvey, 1987; Blair and McPherson, 1998; Kaitna and Huebl, 2013). Individual lobes vary from several decimeters up to 20 m in width and taper down-fan in planview, with abrupt distal fronts ranging from a few centimeters to a few decimeters in height (Fig. 6F–I). Their surface is generally flat and featureless, except for protruding pebbles or cobbles. These deposits are traceable upslope along the main incised channels (RFC), from which they originated as overflows. Propagation within channels prevented lateral expansion and flow thinning, enhancing runout potential. These deposits are very recent, testified by a near absence of clasts bearing signs of weathering.

The recently active sector is incised by a few dry, low-sinuosity channels and washes (RFC) (Fig. 6J–N) that formed by reworking and partial downstream redistribution of the debris-flow deposits by precipitation-

driven runoff from the catchment. Channel profiles broaden and increase in width/depth ratio toward the distal domain, with less prominent margins. Locally, recent mudflow deposits overlie the clast-supported channel bed, indicating recent mass-flow activity within channels and instances of overflow. Dry channel beds consist mostly of poorly organized, clast-supported gravel with a granulometric

range (from centimetric pebbles to meter-sized boulders) identical to that of the surrounding debris-flow-dominated surface. Silt- to granule-size debris is absent from gravel interstices, but forms finer-grained sheets and lobes downstream of inner bends or in more distal, low-gradient channels ($<7^\circ$). The dominance of sporadic but energetic water runoff in configuring channel deposits is testified by (i) crudely

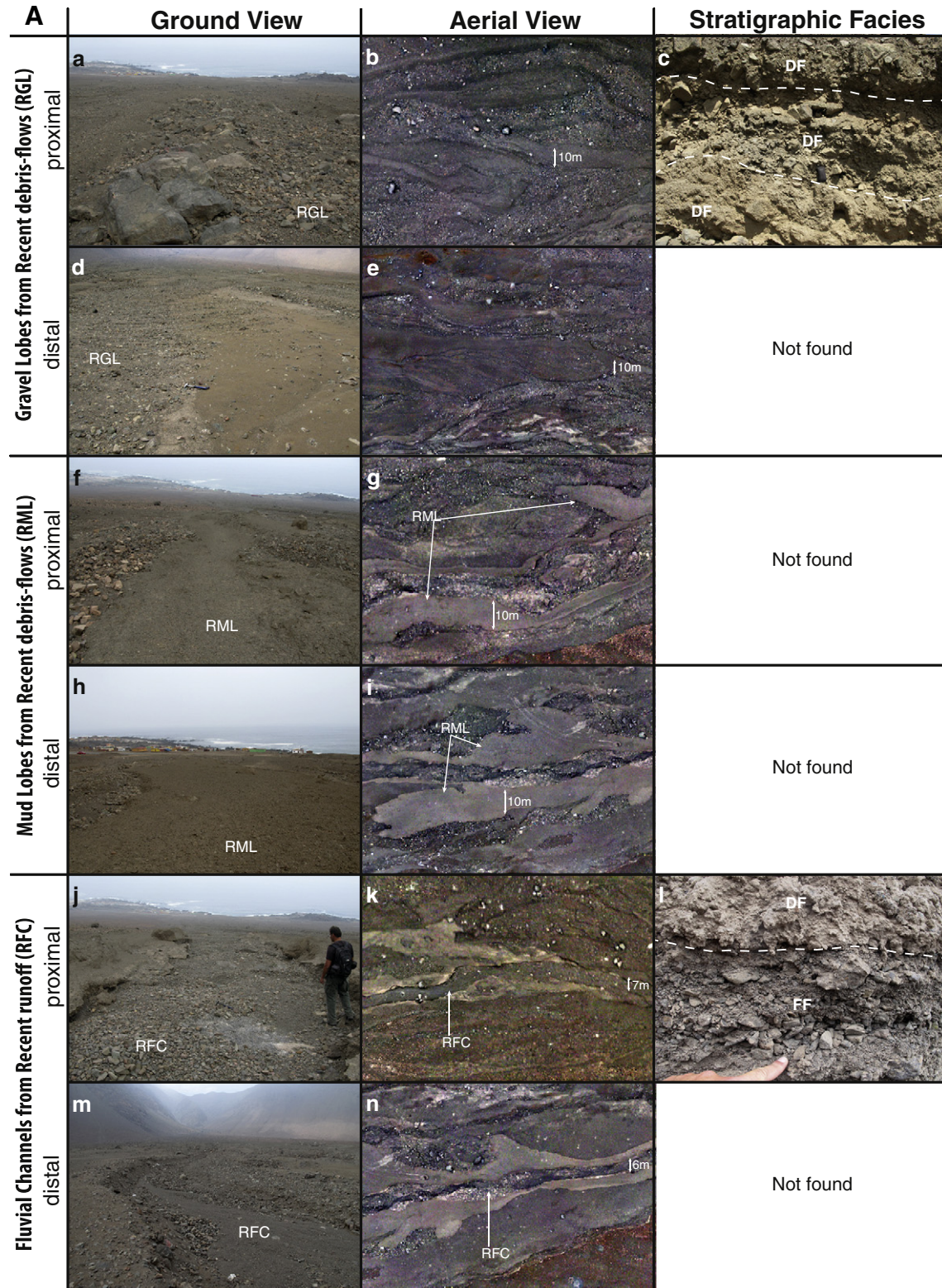


Fig. 6. Morphological facies in ground view, in aerial images and corresponding stratigraphic facies if found. See Fig. 1 for locations of aerial images. Panel l is also part of Fig. 5F and U of Fig. 5E. Contrast of aerial images was optimized for better visibility.




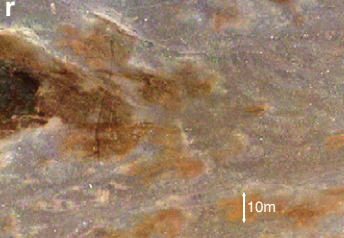

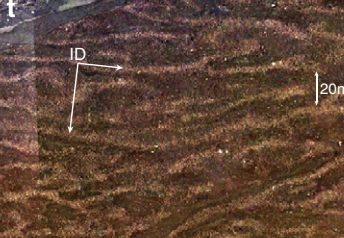
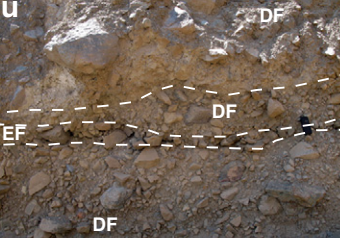
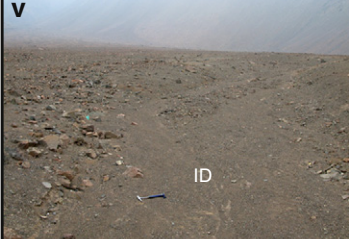
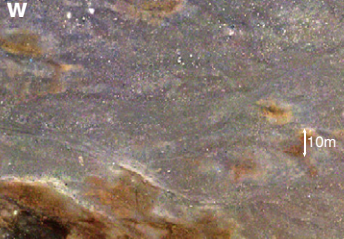
B	Ground View	Aerial View	Stratigraphic Facies
Residual Deposits from past debris-flows (IRD)	o proximal  IRD	p  IRD 9m	Not found
	q distal  IRD	r  10m	Not found
Eroded and Filled Depositions of local runoff (ID)	s proximal  ID	t  ID 20m	u  DF EF DF
	v distal  ID	w  10m	Not found

Fig. 6 (continued).

developed macroforms, such as gravelly lateral bars and longitudinal bars with moderate to good sorting and imbrication (Carling and Reader, 1982; Bluck, 1987; Zielinski, 2003), (ii) well-developed microforms such as gravel clusters (e.g., Brayshaw et al., 1983; Brayshaw, 1984) or transverse clast dams (Bowman, 1977; Church and Jones, 1982; Bluck, 1987), and (iii) reworking of fine sediments to leave a

clast-supported bed distally associated with coarse sandy to fine pebbly deposits where flow competence was decreased.

4.2.2. Inactive fan surface

Most of the inactive fan surface presents an irregular, gently mounded topography that originally formed by debris flows (Fig. 2C,

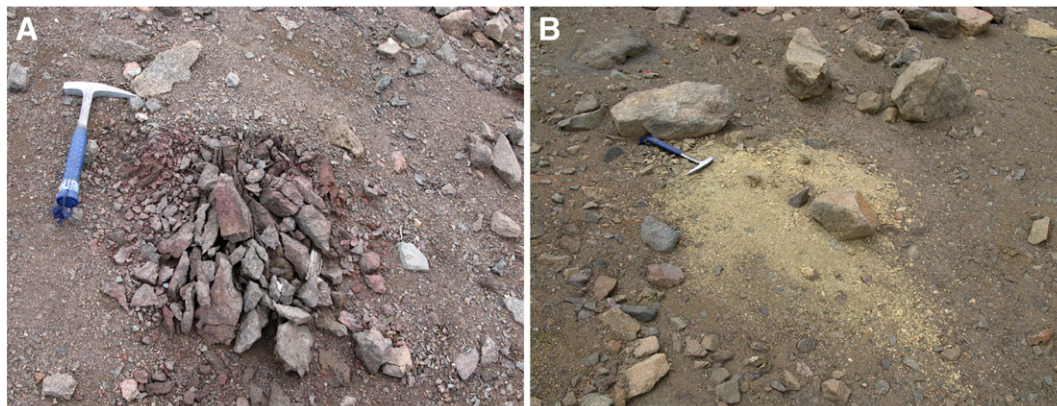


Fig. 7. The effect of salt weathering on clasts. (A) Heavily disintegrated cobble. (B) Completely disintegrated clast (clast ghost).

D), now bearing signs of prolonged exposure to weathering, such as pervasive rock varnish, spalling and exfoliation, and various stages of clast brecciation up to complete disintegration (Fig. 7). Because of intense modification by secondary processes, its surface can only be divided into the following morphological facies: (i) channels that occur in topographic lows originating from the long-term action of secondary runoff (ID) and (ii) residual deposits including the rest of the inactive surface (IRD).

The residual deposits show little relief and textural patterns but present faintly recognizable remnants of debris flows. Their proximal to medial domain mainly consists of a mantle of angular clasts (fine pebbles up to boulders), generally with scarce to no matrix at the surface, but commonly with abundant, poorly sorted silty to granular matrix a few centimeters below the surface (Fig. 6O–R). Radially oriented linear to slightly sinuous and transverse arcuate alignments and segregations of relatively coarser clasts are evident, isolated, or in association as probable remnants of ancient debris-flow lobes. The distal fan domain is covered by a relatively uniform, low-relief mantle of fine gravelly silty sand to sandy silt. Elevated areas are flatter and have a more regular topography than the proximal fan. Prolonged weathering and deflation on the residual surface is evident from a thin, irregular, armor of granules and pebbles, common occurrence of clasts in an advanced stage of disintegration and ‘clast ghosts’ (Fig. 7), slightly hardened salt horizons a few centimeters below the surface, and patterned ground in the form of segregated pebbles and granules in reticular networks.

The inactive fan sector has numerous shallow incisions with depths up to 1 m and widths up to 10 m (ID), formed by long-term intermittent runoff (e.g., Wells and Dohrenwend, 1985; Blair and McPherson, 1994). On the proximal to medial domain of the fan, the dry beds of incisions are covered by openwork (matrix-free) cobble gravel, a few decimeters up to a couple of meters wide and up to 20–30 cm thick (Fig. 6S–U). These elements are often continuous over the entire proximal to medial fan and form multiple, parallel, tributary drainage networks. On the distal fan, dry channel beds consist of accumulated moderately sorted fine gravel and sand (Fig. 6V–W). Coarser cobble-sized debris formed distinctive mesoforms such as clast dams and imbricate gravel clusters, testifying to the action of precipitation-driven runoff (Brayshaw, 1984; Bluck, 1987). The transition from openwork cobble gravel beds on the proximal to medial domain to fine-grained channel fills on the distal domain probably originates from distal in-channel deposition of fine material entrained by runoff on the steeper proximal to medial surface. This hypothesis will be tested in Section 4.4. The color contrast of distal channel fills with the adjacent varnished fan surface demonstrates that these elements have long been the most active locus of geomorphic activity and sedimentation, whereas the main fan surface was undergoing only weathering and erosion. Because of the large apex incision (~15 m wide and ~3 m deep), the source of the runoff on the inactive sector has solely been from direct precipitation on the inactive sector and possibly its adjacent slopes. Therefore, runoff was only able to redistribute fines, in contrast to the active sector where runoff originated from the catchment and thus had larger volume and stream power. This explains the large difference in channel configuration between the active and inactive sectors, where the former (Section 4.2.1) has 2–3 large incised channels and the latter features numerous small channels (Fig. 2).

4.3. Trends in particle size and surface roughness

We compared the proximal and distal fan and the active and inactive sectors for the locations where we defined the morphological facies (Sections 4.2.1–4.2.2, Fig. 8). Mudflow deposits form the finest-grained facies on the active fan surface and occur on relatively high areas (Fig. 9A,B) adjacent to the incised channels as elevated lobes and ridges. There is a significant down-fan decrease in median particle size within the mudflow deposits. The debris-flow sheets and lobes are the coarsest-grained morphological facies and show a down-fan decrease in median particle size resulting from the following combined factors:

- Most coarse material in debris flows is deposited in levees on the proximal fan domain.
- Coarse-grained debris flows have higher internal shear strength and are thus more likely to halt on steeper, proximal slopes; whereas finer-grained debris flows are able to spread onto the distal fan (Whipple and Dunne, 1992).
- Fan width increases downslope, so an increasing percentage of the fan surface has long been inactive and thus subject to protracted weathering and reduction of the surface texture.

The particle size of incised channel surfaces exceeds that of the mudflow deposits but is smaller than that of the debris-flow deposits and does not show any significant fining downstream (Fig. 9A,B).

The proximal domain of the inactive surface (Fig. 9C) shows a clear distinction between the incised and residual surface, based on elevation and median particle size. This is caused by the coarse lags on the incised and depressed inactive surface, whereas the residual, elevated surface comprises finer material with occasional patches of coarse sediments (Figs. 2; 6P,T; 8E). The texture of the incised and residual fan surface fines down-fan on the inactive sector. Moreover, the particle size of the incised and residual surface of the distal fan is approximately equal because of the deposition of fines eroded on the proximal fan. This renders the distinction between channels and adjacent residual surfaces nearly impossible based on aerial images only (Fig. 8).

The inactive fan surface is topographically considerably smoother than the active surface (Fig. 10A–C) because weathering and erosion redistributed debris from elevated to depressed areas. The increased roughness in the most proximal domain is caused by the deep incision in proximity of the apex. In combination with the small fan width, and thus a small sample size, this leads to enhanced roughness values in the apex region. The slight increase of roughness on the distal domain of the inactive sector is an artifact of a slight decrease in DEM quality; in reality roughness values appear to remain relatively constant below 500 m from the apex. The values of detrended elevation and surface roughness on the active surface and particle size on the active and inactive surface strongly decline down-fan (Fig. 10B–C). We interpret this to result from the high yield strength of coarse-grained debris flows compared to the low yield strength of fine-grained, more fluidal flows. Because high-yield-strength debris flows result in deposits with more relief and are coarser grained, surface relief and texture are higher on the proximal domain of the fan. Additionally, the downslope increase in fan width leads to an increase in long inactive areas, as the width of individual debris flows does not increase downslope in a similar proportion. The relative amount of long inactive, and thus more heavily weathered, areas is thus larger on the distal domain of the fan, resulting in a smoother topography averaged over the total fan width. The spatially averaged particle size on the active fan sector is only slightly higher than on the inactive sector of the fan, despite considerable evidence of extensive clast weathering on the latter. We ascribe this to the presence of coarse-grained lags on the inactive sector and to the large extent of recent and fine-grained mudflow deposits on the surface of the active fan sector.

4.4. Effect of slope on fluvial reworking patterns

The channels on the proximal to medial domain of the abandoned fan surface comprise coarse lags of openwork gravel, whereas they comprise fine-gravelly, silty sand to sandy silt on the distal domain (see Section 4.2.2). Steep slopes on the proximal fan promote erosion of relatively fine sediment by runoff and transport toward the distal fan, where reduced gradients favor deposition in depressions and channels caused by a decrease in flow competence. This interpretation is further supported here by a quantification of sediment mobility over a range of slopes.

The transition from erosion of fines by runoff on the proximal to medial domains of the inactive fan surface to redeposition on the distal

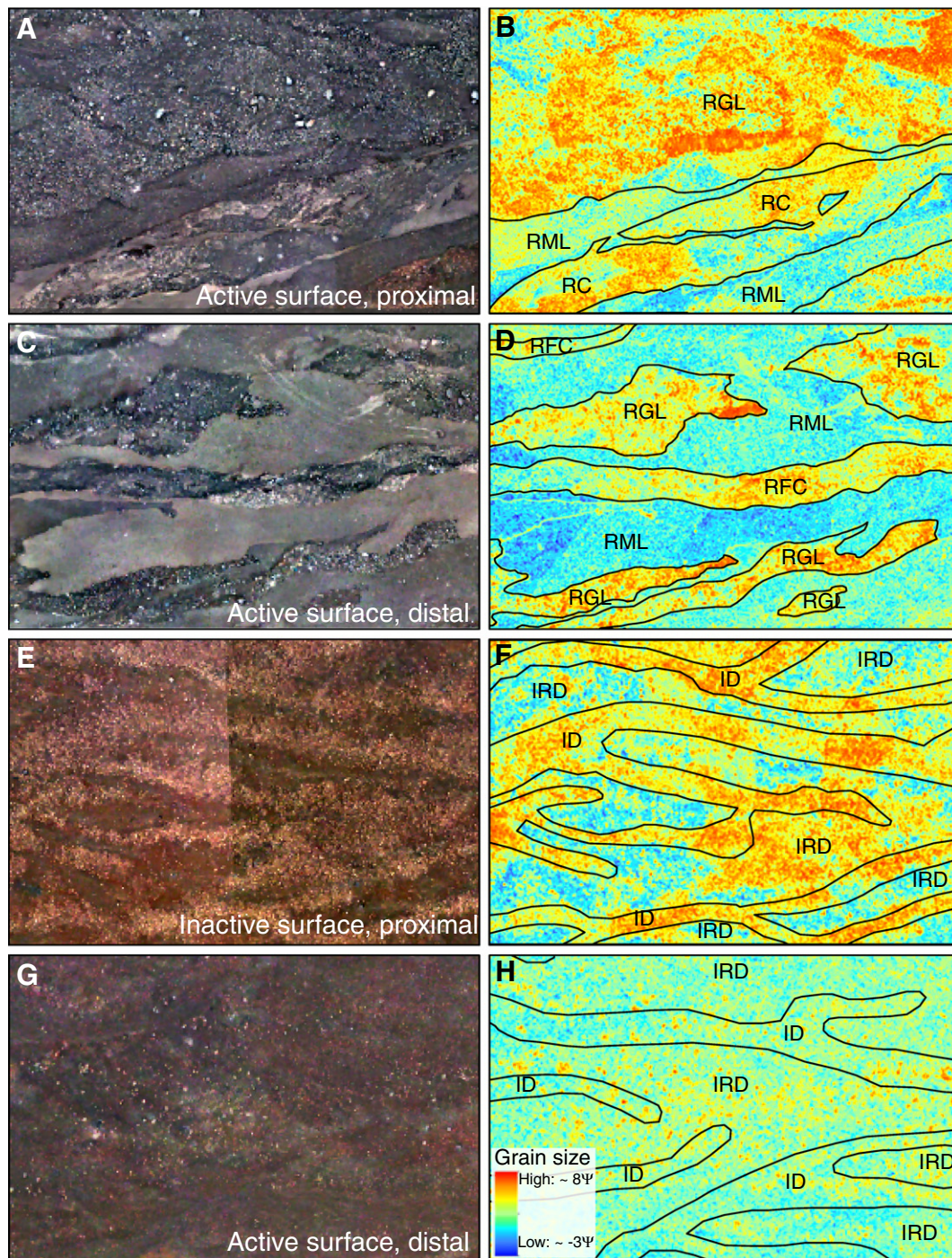


Fig. 8. Particle size-sorting patterns of morphological facies of proximal and distal, active and inactive sectors. Legend for B, D, F, H given in H. See Fig. 1 for locations of the orthophoto subsets. The particle size distributions within the morphological facies are plotted in Fig. 9. Contrast of aerial images was optimized for better visibility.

domain occurs at a gradient of $\sim 7^\circ$. The typical median particle size of these fines, obtained by mechanical sieving, is $\sim 1\psi$ (2 mm). Runoff on the inactive fan surface typically concentrates in depressions or channels ~ 5 m wide and ~ 1 m deep. Assuming a water depth of 0.25 m in these depressions, we calculated both the mobility and threshold for motion of median particle sizes varying from -1ψ (0.5 mm) to 2ψ (4 mm) on a range of slopes (Fig. 11).

The median particle size at which the erosion–deposition transition occurs on a slope of 7° is $\sim 0.5\psi$ (1.4 mm), which is in good agreement with the observed $\sim 1\psi$ (2 mm). Assuming a different water depth does not affect this conclusion significantly: flow depths of 0.125 m and 0.5 m result in erosion–deposition transitions at a surface gradient

of 7° at median particle sizes of $\sim 0.5\psi$ (0.7 mm) and $\sim 1.5\psi$ (2.8 mm), respectively. The good correspondence between the measured particle sizes of the eroded fines with particle sizes predicted by Eq. (3) at a slope of 7° confirms the runoff-related origin of the elongate coarse lags in depressions on the proximal and medial fan. Fines eroded from high proximal gradients are deposited on the distal domain.

4.5. Fan surface evolution after abandonment

The volumetric dominance of debris-flow facies in the stratigraphic sections shows that the studied fan was formed dominantly by debris-flow deposition, while the overall volume of runoff-related facies is

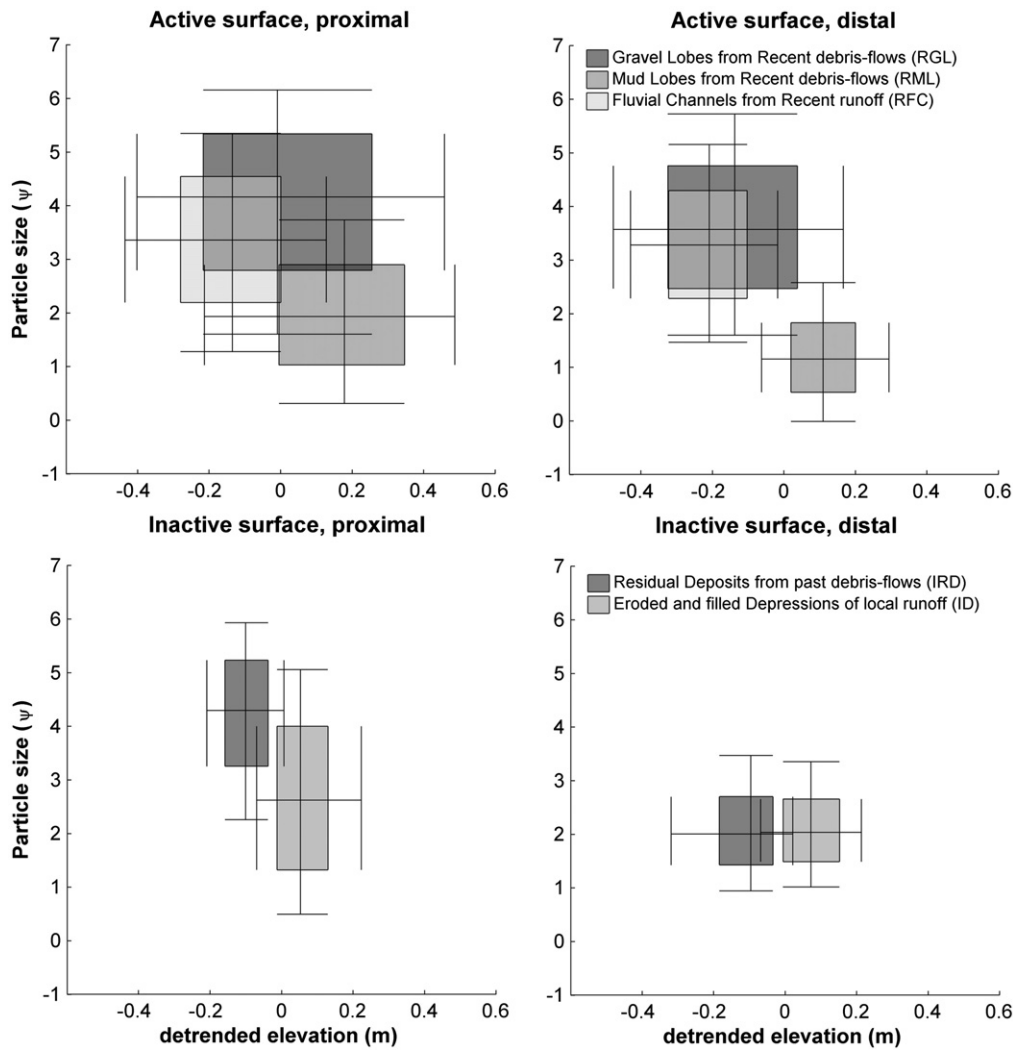


Fig. 9. Differences in combinations of particle size and local relief between morphological facies. The arithmetic median particle diameter (ψ) and elevation (m) above a smooth trend surface (see [Methods](#)) are plotted for morphological facies in representative areas defined in 4 ([Fig. 8](#)). Boxes indicate quartiles, line crossings indicate the median, and whiskers indicate the 10th and 90th percentile.

minor and mainly of secondary origin. This means that aggradation is episodic and rapid and often followed by phases of long inactivity and reworking, which is reflected in the morphology and texture of the active ($M > 1$) and inactive ($M < 1$) fan surface. The former mainly consists of relatively unaltered debris-flow deposits, whereas the original, debris-flow-related, depositional morphology is strongly modified and hardly recognizable on the latter. On the inactive surface, relief is significantly subdued by weathering and erosion, and local runoff redistributes fines.

We provide a detailed conceptual model for the evolution of the fan surface after abandonment, explaining the above findings ([Fig. 12](#)). Initially, the fan surface consists of amalgamated, mostly unaltered, debris-flow deposits and therefore has a coarse-grained texture with significant relief. The active surface ([Fig. 12A](#)) thus represents fans or fan sectors dominated by primary processes of deposition ($M > 1$, Eq. (1)). After abandonment the surface is exposed to weathering, runoff, and deflation ([Fig. 12B](#)). Because of the great availability of moisture and associated salts in the form of coastal fogs ([Eriksen, 1981; Schemenauer and Cereceda, 1992](#)), coarse fan sediments undergo intense breakdown and produce considerable volumes of fines ([Berger, 1993; Berger and Cooke, 1997; Goudie et al., 2002](#)). Part of the finest weathering products is probably deflated, whereas coarser fractions are eroded by runoff from local topographic highs (gravel lobes and levees) into lows (channels and depressions). Runoff erodes laterally

into debris-flow deposits, causing selective entrainment of the supporting matrix and concentration of gravel to form coarse lags along channel margins, where gravel is displaced from overlying debris-flow lobes by rolling, fall, and bank collapse. Fines may temporarily accumulate along channel beds but are ultimately transported down-fan to form finer-grained, distal channel fills. Channel lags form an armor that prevents further incision into the fan surface, whereas the more elevated areas remain subject to erosion and deflation. Through time, this combination of processes leads to a decrease in surface relief and to the redistribution of coarse material from topographic highs to lows on the proximal to medial fan surface, causing textural inversion ([Fig. 12C](#)). Conversely, as fines are mostly deposited rather than eroded in topographic lows on the distal fan, the textural contrast between topographic highs and lows in this domain is gradually reduced ([Fig. 12C](#)). Thus the weathered surface in [Fig. 12C](#) represents fans or fan sectors dominated by secondary processes ($M < 1$).

5. Discussion

5.1. Characteristic time scales of fan surface modification in arid environments

In general, smoothing and gradual fining of long-inactive or abandoned alluvial fan surfaces have been observed in many arid regions,

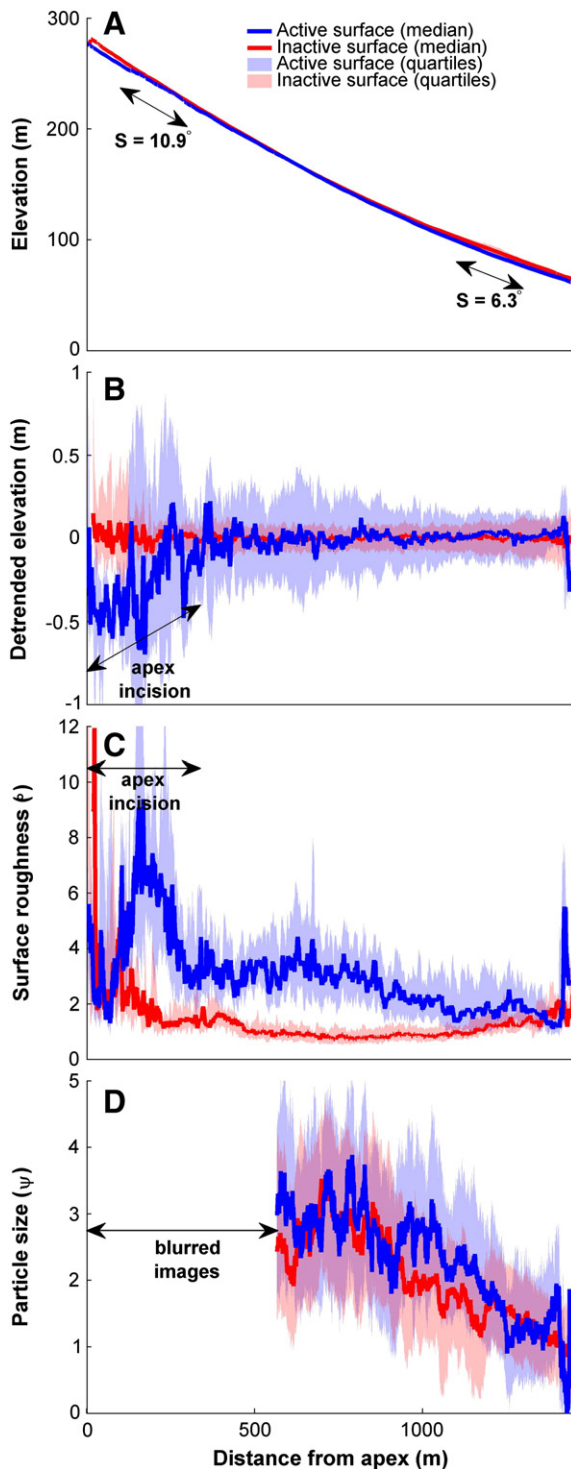


Fig. 10. Down-fan trends of (A) elevation, (B) elevation above the smooth trend surface (detrended elevation), (C) surface roughness (defined by Frankel and Dolan (2007)) and (D) particle size. Inactive sector is smoother than active sector as indicated by detrended elevation and surface roughness. Surface roughness and particle size decrease down-fan and the local variation (shaded) of detrended elevation, surface roughness and particle size also decrease down-fan.

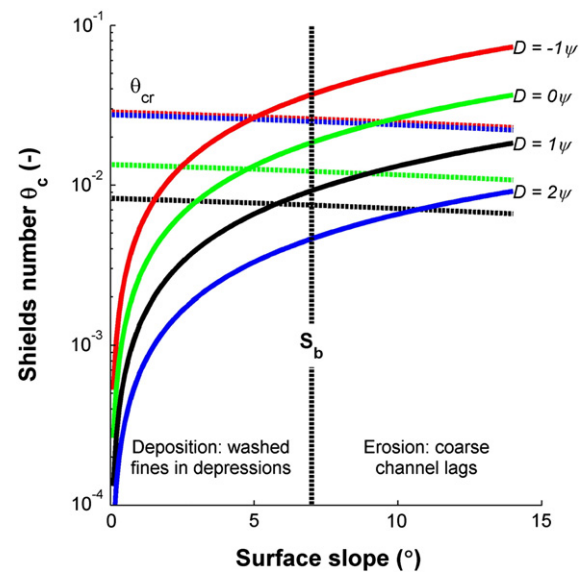


Fig. 11. Potential mobility of sediment explains down-fan sorting patterns. Calculated fluvial sediment mobility (drawn lines) compared to the threshold for sediment motion (dashed lines) expressed as Shields numbers for a range of slopes and characteristic particle sizes using the model of Vollmer and Kleinhans (2007). Intersection of corresponding colors indicates the slope at which deposition could occur. S_b indicates the observed transition from coarse channel lags $>1\phi$ (2 mm) to fines $<1\phi$ deposited in depressions. The proximity of all intersections of the three black lines indicates excellent agreement between the predicted and observed location of transition from coarse channel lags to out-washed fines.

1993; Berger and Cooke, 1997; González et al., 2006; Cortés et al., 2012). Invariably, the combined action of weathering and erosion leads to smoothing of initial bar-and-swale topography and eventually to the development of mature, low-relief desert pavements with a much more subdued topography (e.g., Wells et al., 1987; Ritter et al., 1993; Frankel and Dolan, 2007). Mature desert pavements generally consist of homogeneous, densely packed, gravel-sized surfaces (see pictures in Berger, 1993; Al-Farraj and Harvey, 2000; Frankel and Dolan, 2007). The time required for the development of mature desert pavements depends strongly on location (i.e., climate and lithology). Approximately 100 ky was required for the development of a smooth, mature desert pavement in the Negev Desert (Amit et al., 1993). On the Kyle Canyon fan in southern Nevada, a moderate-stage pavement developed in ~130 ky (Reheis et al., 1992), while ~83 ky was needed for pavement development of noncarbonate lithologies in the Mojave Desert ((Ku et al., 1979), in (Al-Farraj and Harvey, 2000)). In the same desert, a moderately paved fan surface had an age of ~70 ky (Frankel et al., 2007), while completely smooth pavement on fans along the San Andreas fault had an age of 280 ky (Matmon et al., 2006).

Along the Atacama coast of northern Chile, thoroughly smoothed fan surfaces along the Mejillones fault were dated at 35 ky (Cortés et al., 2012); farther inland, smooth fan surfaces dissected by the Atacama fault were dated at 424 ky (González et al., 2006). The relatively young age of 35 ky (Cortés et al., 2012) for smooth fan surfaces along the Mejillones fault (90 km south of the fan studied here) implies that modification rates along the Atacama coast are significantly higher than in most other arid environments. As moisture availability is generally the limiting factor for weathering in arid climates (e.g., Warke, 2013), the cause of rapid fan-surface modification along the Atacama coast is the camanchaca, which provides considerable amounts of moisture and dissolved salts leading to extremely high weathering rates (Eriksen, 1981; Schemenauer and Cereceda, 1992; Berger, 1993; Goudie et al., 2002). This effectively decreases the morphological factor (Eq. (1)) relative to conditions with similar debris-flow activity but lower weathering rates.

such as the Mojave Desert in the United States (Wells et al., 1987; McFadden et al., 1989; Matmon et al., 2006; Frankel and Dolan, 2007), the Negev Desert in Israel (Amit and Gerson, 1986; Gerson and Amit, 1987; Amit et al., 1993), the United Arab Emirates (UAE) (Al-Farraj and Harvey, 2000), and the Atacama Desert of northern Chile (Berger,

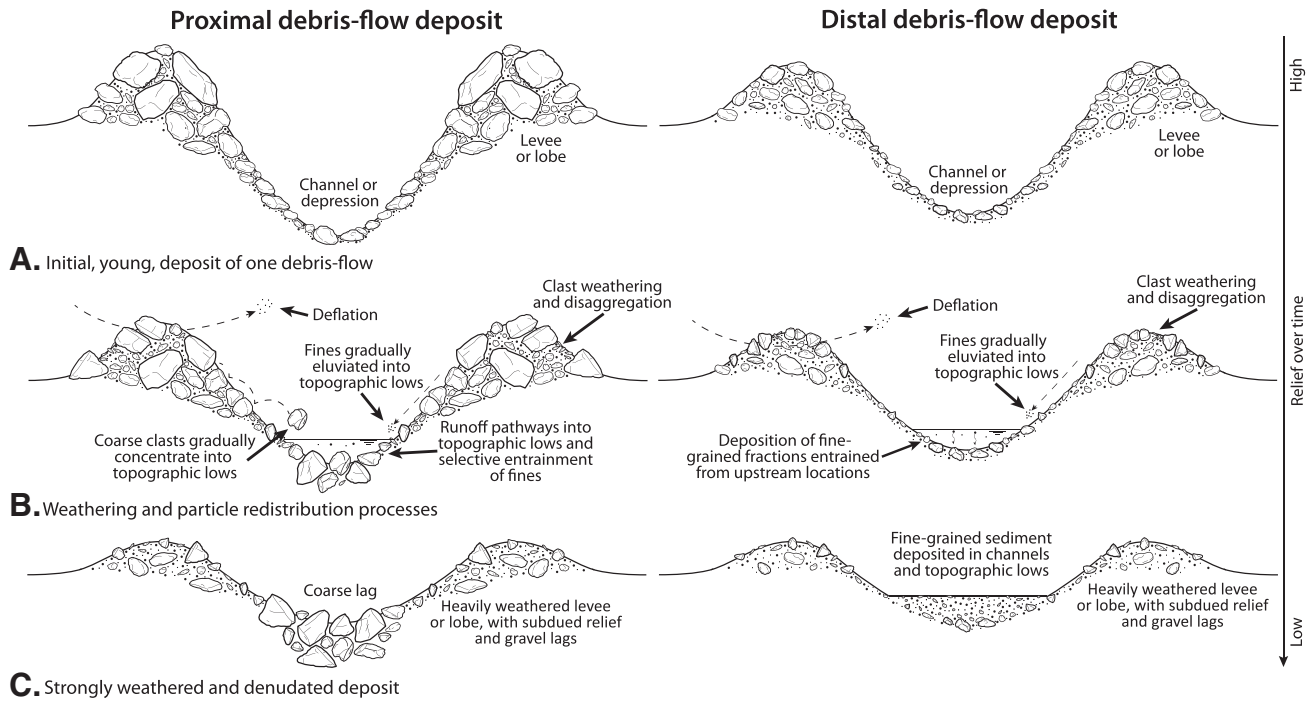


Fig. 12. Conceptual model of the effects of weathering and fluvial reworking on fan-surface texture and morphology for the proximal and distal domains of the fan surface. The fresh surface (A) represents fans or fan sectors dominated by primary processes of deposition ($M > 1$, Eq. (1)) (facies RGL and RML) whereas the weathered surface (C) represents fans or fan sectors dominated by secondary processes ($M < 1$) spanning local disintegration and winnowing to downslope fluvial transport of fines (levees correspond to morphological facies IRD and the channels to ID).

Surprisingly, the high weathering rate prevents surface stabilization. The regular occurrence of the camanchaca interferes with the development of mature desert pavement as it causes particle breakdown below the gravel range, which would otherwise allow the formation of a mechanically stable desert pavement. The resulting fines are easily removed by wind and runoff. Furthermore, the inactive sector of the studied fan differs from relict fan surfaces in other arid environments by the presence of elongate, coarse-grained lags connected into multiple, parallel, tributive drainage patterns over the proximal and medial domains. Previous studies of relict fan surfaces have been carried out on systems aggraded by runoff processes, or mixed runoff and mass-flow processes, with slopes ranging between 1 and 5° (Wells et al., 1987; McFadden et al., 1989; Ritter et al., 1993; Al-Farraj and Harvey, 2000; Matmon et al., 2006; Frankel and Dolan, 2007). Because of this relatively low slope, the local runoff was probably inadequate for removal of fines and formation of fully armored channel lags, whereas on the steeper fan examined here such textural elements are a major surface feature (Figs. 1, 2, 11).

The evidence discussed above shows that the degree of fan stabilization depends on the balance of frequency and magnitude of precipitation on the one hand and on the weathering intensity on the other. In transport-limited, hyperarid environments where geomorphologically effective events are rare ($M < 1$), particularly high weathering rates may prepare relict fan deposits for partial entrainment by lesser and thus relatively more frequent hydrologic events so that the surface attains a fluvial morphological imprint. The stabilization of fans in weathering-prone arid settings may thus not only require the formation of a coarse surface pavement resistant to physical transport, but also a bedrock lithology/mineralogy resilient to disaggregation by weathering.

5.2. Implications for recognition of primary formative process in imagery

Alluvial fans on Mars are ubiquitous and potential sources of information on past hydrological conditions depending on the amount of

water involved in the primary formative process. Hence detailed analyses of aerial and satellite imagery on terrestrial and Martian fans often aim at the identification of formative processes based on morphological features (e.g., Hooke, 1987; Whipple and Dunne, 1992; Blair and McPherson, 1998; Gómez-Villar and García-Ruiz, 2000; Blair, 2002; Moore and Howard, 2005; Frankel and Dolan, 2007; Volker et al., 2007; Kleinhans, 2010; Ferrier and Pope, 2012). For example, the presence or absence of levees and depositional lobes was used to assert whether Martian fans are of fluvial or debris-flow origin (e.g., Dickson and Head, 2009; Reiss et al., 2011). However, our work and literature clearly demonstrate that fan-surface morphology and texture are often determined by secondary rather than primary processes, and this is particularly the case in environments with prolonged inactivity of primary formative processes such as planet Mars (Reiss et al., 2004; Schon et al., 2009; Carr and Head, 2010; Mangold et al., 2012; de Haas et al., 2013). In such settings the degree of surface smoothing and pavement development must be interpreted with extreme caution, especially because alluvial fan surfaces can be severely modified within a few thousands of years (Frankel and Dolan, 2007). Our study demonstrates that steep, debris-flow-dominated fan surfaces can effectively be masked by a well-developed drainage pattern that would suggest a runoff origin from aerial images. Therefore, determination of fan formative processes based solely on surface morphological traits is potentially highly misleading, can be severely hindered by surface reworking within a few thousands of years following a major phase of aggradation, and becomes more and more problematic with increasing age. This conclusion confirms the long-debated statement by Blair and McPherson (1994) that the origin of alluvial fans has been often misinterpreted as the occurrence of well-developed drainage networks on alluvial-fan surfaces is not diagnostic for dominant aggradation by runoff.

In addition to surface modification by weathering and fluvial processes, fan surfaces can also be heavily modified by aeolian processes. The fan studied here is relatively sheltered and therefore subject to only minor deflation, but aeolian reworking and modification of fan

surfaces are common in many other arid environments (Anderson and Anderson, 1990; Blair et al., 1990; Blair and McPherson, 1992), potentially leading to heavily deflated surfaces with inverted channels (e.g., Morgan et al., 2014). The identification of fan-formative processes from aerial images should therefore always be accompanied by an assessment of the morphological factor M : the ratio of the time to build morphology by primary processes versus the time to modify, rework, and erase morphology by secondary processes. The formative processes on fans subject to low M values should then be inferred from a combination of multiple approaches whenever possible, including sedimentological outcrop analysis and morphometrics. Furthermore, it remains conceivable that the morphological and size-sorting patterns of the primary processes are still observable as a palimpsest or blueprints underlying the patterns caused by secondary processes. This emphasizes the need for quantification of pattern characteristics to identify and discriminate between morphological and textural characteristics resulting from primary and secondary processes.

6. Conclusions

We studied the relative effectiveness of primary processes of deposition and secondary weathering and fluvial erosion in forming the stratigraphy, surface morphology, and texture of an alluvial fan along the Atacama Desert coast. The bipartite morphology of the studied fan, with sharp morpho-sedimentary contrast between the active and inactive parts, allowed independent study of the morphological and textural characteristics on both fan sectors. Based on hyperspatial imagery and field data, we conclude that:

- The surface morphology and texture on the inactive sector are predominantly of secondary fluvial origin with strong down-fan fining imprinted over original debris-flow morphology.
- Such fluvial deposits are hardly preserved in the subsurface, where debris-flow deposits are volumetrically dominant, indicating long-term aggradation by debris flow.
- Salt-weathering and secondary fluvial erosion reduce surface morphology and relief on the inactive sector. Moreover, they cause inversion of the original surface texture patterns formed by debris flows on the steep proximal to medial domain of the inactive sector. The initially coarse levees are reduced in particle size, while precipitation-driven runoff is concentrated in former debris-flow channels and depressions, forming coarse lag deposits.
- The aggressive salt-weathering regime along the Atacama coast causes particle breakdown to continue below the gravel size range that would otherwise form a desert pavement. This allows partial entrainment and transport by relatively small and frequent hydrologic events, thus forming a mask of fluvial morphology over a debris-flow-dominated fan.

These results imply that the interpretation of formative processes solely based on imagery is risky as the surface modification of long-inactive fans by weathering and runoff masks the original formative processes. Here, fan surface susceptibility to secondary reworking depends on the ratio of the time to form deposits and relief by primary processes and the time to remove, rework, and form relief by secondary processes. Comparison with stabilized fans reported in literature suggests that the degree of fluvial reworking or stabilization of the surface by a pavement (expressed as a morphological factor M) depends on the lithology and weathering rate, the frequency and magnitude of runoff events and the fan slope, which determine the transportability of the weathered surface sediment.

Acknowledgments

The Matlab code for image entropy calculation is available from the authors upon request. This work is part of the Ph.D. research of TdH, supported by the Netherlands Organisation for Scientific Research (NWO)

and the Netherlands Space Office (NSO) (grant ALW_GO_PL17_2012 to MGK). We gratefully acknowledge Steven de Jong for the feedback and Wouter Marra for the help during fieldwork, and Durham University for the use and operation of the UAV. Constructive comments by two anonymous reviewers and editor Richard Marston are gratefully acknowledged. The authors contributed in the following proportions to conception and design, data collection, analysis and conclusions, and manuscript preparation: TdH(40,50,40,50%), DV(10,20,30,20%), PEC(10,30,10,10%), MGK(40,0,20,20%).

References

- Agisoft, 2011. Image-Based 3D Modelling. Available at: www.agisoft.ru.
- Al-Farraj, A., Harvey, A.M., 2000. Desert pavement characteristics on wadi terrace and alluvial fan surfaces: Wadi Al-Bih, U.A.E. and Oman. *Geomorphology* 35 (34), 279–297.
- Amit, R., Gerson, R., 1986. The evolution of holocene reg (gravelly) soils in deserts: an example from the dead sea region. *Catena* 13 (12), 59–79.
- Amit, R., Gerson, R., Yaalon, D., 1993. Stages and rate of the gravel shattering process by salts in desert reg soils. *Geoderma* 57 (3), 295–324.
- Anderson, S.P., Anderson, R.S., 1990. Debris-flow benches: dune-contact deposits record paleo-sand dune positions in north Panamint Valley, Inyo County, California. *Geology* 18 (6), 524–527.
- Araveni, K., Suzuki, O., Pollastri, A., 1989. Coastal fog and its relation to groundwater in the IV region of northern Chile. *Chem. Geol.* 79, 83–91.
- Armijo, R., Thiele, R., 1990. Active faulting in northern Chile: ramp stacking and lateral decoupling along a subduction plate boundary. *Earth Planet. Sci. Lett.* 98 (1), 40–61.
- Berger, L.A., 1993. Salts and Surface Weathering Features on Alluvial Fans in Northern Chile. (Ph.D. thesis) University College London.
- Berger, L.A., Cooke, R.U., 1997. The origin and distribution of salts on alluvial fans in the Atacama Desert, northern Chile. *Earth Surf. Process. Landf.* 22 (6), 581–600.
- Blair, T.C., 1999. Sedimentology of the debris-flow-dominated Warm Spring Canyon alluvial fan, Death Valley, California. *Sedimentology* 46 (5), 941–965.
- Blair, T.C., 2002. Alluvial-fan sedimentation from a glacial-outburst flood, Lone Pine, California, and contrasts with meteorological flood deposits. *Flood and Megaflood Processes and Deposits: Recent and Ancient Examples*. IAS Special Publication, pp. 113–140.
- Blair, T.C., McPherson, J.G., 1992. The Trollheim alluvial fan and facies model revisited. *Geol. Soc. Am. Bull.* 104 (6), 762–769.
- Blair, T.C., McPherson, J.G., 1994. Alluvial fans and their natural distinction from rivers based on morphology, hydraulic processes, sedimentary processes, and facies assemblages. *J. Sediment. Res.* 64A, 450–489.
- Blair, T.C., McPherson, J.G., 1998. Recent debris-flow processes and resultant form and facies of the Dolomite alluvial fan, Owens Valley, California. *J. Sediment. Res.* 68 (5), 800–818.
- Blair, T.C., McPherson, J.G., 2009. Processes and forms of alluvial fans. In: Parsons, A., Abrahams, A. (Eds.), *Geomorphology of Desert Environments*. Springer, Netherlands, pp. 413–467.
- Blair, T.C., Clark, J.S., Wells, S.G., 1990. Quaternary continental stratigraphy, landscape evolution, and application to archeology: Jarilla piedmont and Tularosa graben floor, White Sands Missile Range, New Mexico. *Geol. Soc. Am. Bull.* 102 (6), 749–759.
- Blott, S.J., Pye, K., 2001. GRADISTAT: a grain size distribution and statistics package for the analysis of unconsolidated sediments. *Earth Surf. Process. Landf.* 26 (11), 1237–1248.
- Bluck, B., 1987. Bed forms and clast size changes in gravel-bed rivers. *River Channels: Environment and Process*. Blackwell, Oxford pp. 159–178.
- Bowman, D., 1977. Stepped-bed morphology in arid gravelly channels. *Geol. Soc. Am. Bull.* 88 (2), 291–298.
- Brayshaw, A.C., 1984. Characteristics and origin of cluster bedforms in coarse-grained alluvial channels. *Sedimentology of Gravels and Conglomerates*, 10 pp. 77–85.
- Brayshaw, A.C., Frostick, L.E., Reid, I., 1983. The hydrodynamics of particle clusters and sediment entrapment in coarse alluvial channels. *Sedimentology* 30 (1), 137–143.
- Carbonneau, P.E., 2005. The threshold effect of image resolution on image-based automated grain size mapping in fluvial environments. *Earth Surf. Process. Landf.* 30 (13), 1687–1693.
- Carbonneau, P.E., Lane, S.N., Bergeron, N.E., 2004. Catchment-scale mapping of surface grain size in gravel bed rivers using airborne digital imagery. *Water Resour. Res.* 40 (7), W07202 (Jul).
- Carbonneau, P., Fonstad, M.A., Marcus, W.A., Dugdale, S.J., 2012a. Making riverscapes real. *Geomorphology* 137 (1), 74–86 Geospatial Technologies and Geomorphological Mapping Proceedings of the 41st Annual Binghamton Geomorphology Symposium.
- Carbonneau, P.E., Piégay, H., Lejot, J., Dunford, R., Michel, K., 2012b. Hyperspatial imagery in riverine environments. *Fluvial Remote Sens. Sci. Manag.* 163–191.
- Carling, P.A., Reader, N.A., 1982. Structure, composition and bulk properties of upland stream gravels. *Earth Surf. Process. Landf.* 7 (4), 349–365.
- Carr, M.H., Head, J.W., 2010. Geologic history of Mars. *Earth Planet. Sci. Lett.* 294 (34), 185–203.
- Church, M., Jones, D., 1982. Channel bars in gravel-bed rivers. *Gravel-bed rivers* pp. 291–338.
- Cortés, A.J., González, L.G., Binnie, S.A., Robinson, R., Freeman, S.P.H.T., Vargas, E.G., 2012. Paleoseismology of the Mejillones Fault, northern Chile: insights from cosmogenic ¹⁰Be and optically stimulated luminescence determinations. *Tectonics* 31 (2) (n/a–n/a).
- de Haas, T., Hauber, E., Kleinhans, M.G., 2013. Local late Amazonian boulder breakdown and denudation rate on Mars. *Geophys. Res. Lett.* 40 (14), 3527–3531.
- de Villiers, G., 2013. Delta and Fan Morphologies on Mars as Climate Indicators. (Ph.D. thesis) Utrecht University, Faculty of Geosciences, Department of Physical Geography.

- Dickson, J.L., Head, J.W., 2009. The formation and evolution of youthful gullies on Mars: gullies as the late-stage phase of Mars most recent ice age. *Icarus* 204 (1), 63–86.
- Dunai, T.J., López, G.A.G., Juez-Larr, J., 2005. Oligocene–Miocene age of aridity in the Atacama Desert revealed by exposure dating of erosion-sensitive landforms. *Geology* 33 (4), 321–324.
- Eriksen, G.E., 1981. Geology and origin of Chilean nitrate deposits. *U. S. Geol. Surv. Prof. Pap.* 1188, 1–37.
- Ferraris, B.F., Di Biase, F.F., 1978. Explanatory Notes Sheet N.30 (1:250,000), Hoja Antofagasta, Carta Geológica de Chile. Tech. rep., El Instituto Nacional de Investigaciones Geológicas de Chile, Santiago.
- Ferrier, G., Pope, R.J., 2012. Quantitative mapping of alluvial fan evolution using ground-based reflectance spectroscopy. *Geomorphology* 175, 14–24.
- Fisher, R.V., 1971. Features of coarse-grained, high-concentration fluids and their deposits. *J. Sediment. Res.* 41 (4), 916–927.
- Fonstad, M.A., Dietrich, J.T., Courville, B.C., Jensen, J.L., Carbonneau, P.E., 2013. Topographic structure from motion: a new development in photogrammetric measurement. *Earth Surf. Process. Landf.* 38 (4), 421–430.
- Frankel, K.L., Dolan, J.F., 2007. Characterizing arid region alluvial fan surface roughness with airborne laser swath mapping digital topographic data. *J. Geophys. Res.* 112 (F2), F02025.
- Frankel, K.L., Brantley, K.S., Dolan, J.F., Finkel, R.C., Klinger, R.E., Knott, J.R., Machette, M.N., Owen, L.A., Phillips, F.M., Slate, J.L., Wernicke, B.P., 2007. Cosmogenic ^{10}Be and ^{36}Cl geochronology of offset alluvial fans along the northern Death Valley fault zone: implications for transient strain in the eastern California shear zone. *J. Geophys. Res.* 112 (B6) (n/a–n/a).
- Gerson, R., Amit, R., 1987. Rates and modes of dust accretion and deposition in an arid region the Negev, Israel. *Geol. Soc. Lond., Spec. Publ.* 35, 157–169.
- Gómez-Villar, A., García-Ruiz, J., 2000. Surface sediment characteristics and present dynamics in alluvial fans of the central Spanish Pyrenees. *Geomorphology* 34 (34), 127–144.
- González, L.G., Dunai, T., Carrizo, D., Allmendinger, R., 2006. Young displacements on the Atacama Fault System, northern Chile from field observations and cosmogenic ^{21}Ne concentrations. *Tectonics* 25 (3) (n/a–n/a).
- Goudie, A.S., Wright, E., Viles, H.A., 2002. The roles of salt (sodium nitrate) and fog in weathering: a laboratory simulation of conditions in the northern Atacama Desert, Chile. *Catena* 48 (4), 255–266.
- Haralick, R.M., Shapiro, L.G., 1985. Image segmentation techniques. *Comput. Vision Graph. Image Process.* 29 (1), 100–132.
- Hartley, A.J., Mather, A.E., Jolley, E., Turner, P., 2005. Climatic controls on alluvial-fan activity, Coastal Cordillera, northern Chile. *Alluvial Fans: Geomorphology, Sedimentology, Dynamics*. Geological Society London Special Publication, pp. 95–115.
- Harvey, A.M., 2010. Local buffers to the sediment cascade: debris cones and alluvial fans. *Sediment Cascades: An Integrated Approach*. John Wiley & Sons, Ltd. pp. 153–180.
- Hooke, R., 1987. Mass movement in semi-arid environments and the morphology of alluvial fans. *Slope Stability*. John Wiley & Sons Ltd. pp. 505–529.
- Houston, J., 2006. The great Atacama flood of 2001 and its implications for Andean hydrology. *Hydrol. Process.* 20 (3), 591–610.
- Houston, J., Hartley, A.J., 2003. The central Andean west-slope rainshadow and its potential contribution to the origin of hyper-aridity in the Atacama Desert. *Int. J. Climatol.* 23 (12), 1453–1464.
- Hubert, J.F., Filipov, A.J., 1989. Debris-flow deposits in alluvial fans on the west flank of the White Mountains, Owens Valley, California, USA. *Sediment. Geol.* 61 (3), 177–205.
- Johnson, C., Kokelaar, B., Iverson, R., Logan, M., LaHusen, R., Gray, J., 2012. Grain-size segregation and levee formation in geophysical mass flows. *J. Geophys. Res. Earth Surf.* 117 (F1) (2003–2012).
- Kaitna, R., Huebl, J., 2013. Silent witnesses for torrential processes. *Dating Torrential Processes on Fans and Cones*. Springer, pp. 111–130.
- Kleinhaus, M.G., 2010. A tale of two planets: geomorphology applied to Mars' surface, fluvio-deltaic processes and landforms. *Earth Surf. Process. Landf.* 35 (1), 102–117.
- Kleinhaus, M.G., van Rijn, L.C., 2002. Stochastic prediction of sediment transport in sand-gravel bed rivers. *J. Hydraul. Eng.* 128 (4), 412–425.
- Ku, T.L., Bull, W.B., Freeman, S.T., Knauss, K.G., 1979. Th^{230} – U^{234} dating of pedogenic carbonates in gravelly desert soils of Vidal Valley, southeastern California. *Geol. Soc. Am. Bull.* 90, 1063–1073.
- Major, J.J., 1998. Pebble orientation on large, experimental debris-flow deposits. *Sediment. Geol.* 117 (34), 151–164.
- Mangold, N., Kite, E., Kleinhaus, M., Newsom, H., Ansan, V., Hauber, E., Kraal, E., Quantin, C., Tanaka, K., 2012. The origin and timing of fluvial activity at Eberswalde crater, Mars. *Icarus* 220 (2), 530–551.
- Marchant, M., Cecioni, A., Figueroa, S., Gonzalez, H., Giglio, S., Hebbeln, D., Kaiser, J., Lamy, F., Mohtadi, M., Pineda, V., Romero, O., 2007. Marine geology, oceanography and climate. *The Geology of Chile*. The Geological Society, London pp. 289–308.
- Matmon, A., Nichols, K., Finkel, R., 2006. Isotopic insights into smoothening of abandoned fan surfaces, Southern California. *Quat. Res.* 66 (1), 109–118.
- McFadden, L.D., Ritter, J.B., Wells, S.G., 1989. Use of multiparameter relative-age methods for age estimation and correlation of alluvial fan surfaces on a desert piedmont, eastern Mojave Desert, California. *Quat. Res.* 32 (3), 276–290.
- Moore, J.M., Howard, A.D., 2005. Large alluvial fans on Mars. *J. Geophys. Res. Planets* 110 (E4) (n/a–n/a).
- Morgan, A., Howard, A., Hobley, D.E., Moore, J.M., Dietrich, W.E., Williams, R.M., Burr, D.M., Grant, J., Wilson, S., Matsubara, Y., 2014. Sedimentology and climatic environment of alluvial fans in the Martian Sahel crater and a comparison with terrestrial fans in the Atacama Desert. *Icarus* 229, 131–156.
- Nemec, W., Muszynski, A., 1982. Volcaniclastic alluvial aprons in the Tertiary of Sofia district (Bulgaria). *Rocz. Pol. Towarz. Geol.* 52, 239–303.
- Nishiizumi, K., Caffee, M., Finkel, R., Brimhall, G., Mote, T., 2005. Remnants of a fossil alluvial fan landscape of Miocene age in the Atacama Desert of northern Chile using cosmogenic nuclide exposure age dating. *Earth Planet. Sci. Lett.* 237 (34), 499–507.
- Parker, G., Sutherland, A., 1990. Fluvial armor. *J. Hydraul. Res.* 28 (5), 529–544.
- Pierston, T., 1986. Flow behavior of channelized debris flows, Mount St. Helens, Washington. *Hillslope Processes* pp. 269–296.
- Rees, A., 1968. The production of preferred orientation in a concentrated dispersion of elongated and flattened grains. *J. Geol.* 457–465.
- Reheis, M.C., Sowers, J.M., Taylor, E.M., McFadden, L.D., Harden, J.W., 1992. Morphology and genesis of carbonate soils on the Kyle Canyon fan, Nevada, U.S.A. *Geoderma* 52 (34), 303–342.
- Reiss, D., van Gasselt, S., Neukum, G., Jaumann, R., 2004. Absolute dune ages and implications for the time of formation of gullies in Nirgal Vallis, Mars. *J. Geophys. Res. Planets* 109 (E6) (n/a–n/a).
- Reiss, D., Hauber, E., Hiesinger, H., Jaumann, R., Trauth, F., Preusker, F., Zanetti, M., Ulrich, M., Johnsson, A., Johansson, L., et al., 2011. Terrestrial gullies and debris-flow tracks on Svalbard as planetary analogs for Mars. *Geol. Soc. Am. Spec. Pap.* 483, 165–175.
- Ritter, J., Miller, J., Enzel, Y., Howes, S., Nadon, G., Grubb, M., Hoover, K., Olsen, T., Reneau, S., Sack, D., Summa, C., Taylor, I., Touyinhthiphonexay, K., Yodis, E., Schneider, N., Ritter, D., Wells, S., 1993. Quaternary evolution of Cedar Creek alluvial fan, Montana. *Geomorphology* 8 (4), 287–304.
- Schemenauer, R.S., Cereceda, P., 1992. The quality of fog water collected for domestic and agricultural use in Chile. *J. Appl. Meteorol.* 31, 275–290.
- Schon, S.C., Head, J.W., Fassett, C.I., 2009. Unique chronostratigraphic marker in depositional fan stratigraphy on Mars: evidence for ca. 1.25 Ma gully activity and surficial meltwater origin. *Geology* 37, 207–210.
- Todd, S.P., 1989. Stream-driven, high-density gravelly traction carpets: possible deposits in the Trabeg Conglomerate Formation, SW Ireland and some theoretical considerations of their origin. *Sedimentology* 36 (4), 513–530.
- Todd, S.P., 1996. Process deduction from fluvial sedimentary structures. *Advances in Fluvial Dynamics and Stratigraphy*. Wiley, Chichester pp. 299–350.
- Vargas, G., Ortlieb, L., Rutllant, J., 2000. Aluviones históricos en Antofagasta y su relación con eventos El Niño/Oscilación del Sur. *Rev. Geol. Chile* 27, 157–176.
- Vargas, G., Rutllant, J., Ortlieb, L., 2006. ENSO tropical–extratropical climate teleconnections and mechanisms for Holocene debris flows along the hyperarid coast of western South America (17°–24°S). *Earth Planet. Sci. Lett.* 249 (34), 467–483.
- Volker, H., Waskiewicz, T., Ellis, M., 2007. A topographic fingerprint to distinguish alluvial fan formative processes. *Geomorphology* 88 (12), 34–45.
- Vollmer, S., Kleinhaus, M.G., 2007. Predicting incipient motion, including the effect of turbulent pressure fluctuations in the bed. *Water Resour. Res.* 43 (5) (n/a–n/a).
- Vuille, M., 1999. Atmospheric circulation over the Bolivian Altiplano during dry and wet periods and extreme phases of the Southern Oscillation. *Int. J. Climatol.* 19 (14), 1579–1600.
- Warke, P., 2013. *Weathering in arid regions. Treatise on Geomorphology*, vol. 4. Elsevier pp. 197–227.
- Wells, S.G., Dohrenwend, J.C., 1985. Relict sheetflood bed forms on late Quaternary alluvial-fan surfaces in the southwestern United States. *Geology* 13 (7), 512–516.
- Wells, S.G., Harvey, A.M., 1987. Sedimentologic and geomorphic variations in storm-generated alluvial fans, Howgill Fells, northwest England. *Geol. Soc. Am. Bull.* 98 (2), 182–198.
- Wells, S.G., McFadden, L.D., Dohrenwend, J.C., 1987. Influence of late Quaternary climatic changes on geomorphic and pedogenic processes on a desert piedmont, Eastern Mojave Desert, California. *Quat. Res.* 27 (2), 130–146.
- Whipple, K.X., Dunne, T., 1992. The influence of debris-flow rheology on fan morphology, Owens Valley, California. *Geol. Soc. Am. Bull.* 104 (7), 887–900.
- Whiting, P.J., Dietrich, W.E., Leopold, L.B., Drake, T.G., Shreve, R.L., 1988. Bedload sheets in heterogeneous sediment. *Geology* 16 (2), 105–108.
- Zielinski, T., 2003. Catastrophic flood effects in alpine/foothill fluvial system (a case study from the Sudetes Mts, SW Poland). *Geomorphology* 54 (3), 293–306.